CURRENT STUDIES IN THE LABRADOR CURRENT WITH RESPECT TO THE MOTION OF ICEBERGS

WILSON E. RUSSELL

CURRENT STUDIES IN THE LABRADOR CURRENT WITH RESPECT TO THE MOTION OF ICEBERGS

by

© Wilson E. Russell, M.Sc.

Submitted in partial fulfilment
of the requirements for the degree of Master of Engineering
Memorial University of Newfoundland

March, 1973

CONTENTS

ABSTRACT		iii
I	INTRODUCTION	1
II	EXPERIMENTAL PROCEDURE	4
	2.1 Current Measuring Instrumentation	4
	2.2 The Experimental Method	4
	2.3 Data Reduction	6
III	EXPERIMENTAL RESULTS AND DISCUSSION	8
	3.1 Current-Velocity versus Time Curves for the Near-Surface Sub-Station	8
	3.2 Theoretical Considerations	10
	3.3 Current-Velocity versus Time Curves for Sub-Stations along a Vertical Line	14
	3.4 Current Velocity at Sub-Station A1	16
	3.5 Spatial Correlations	17
	3.6 Some Aspects of Iceberg Drift	21
IV	GEOSTROPHIC CURRENTS	24
	4.1 A Brief Outline of the Theory of the Dynamic Method of Computing Geostrophic Currents	25
	4.2 Determination of the Zero Reference Level	26
	4.3 Calculations	27
	4.4 Discussion with Respect to Results of Chapter 3	30

CONCLUSIONS 32

APPENDIX 33

ACKNOWLEDGMENTS 34

REFERENCES 35

TABLES 36

DIAGRAMS 42

ABSTRACT

Currents were measured in an area of the Labrador current off the Coast of Newfoundland. The measurements were made at four stations over a period of three days. Three of the stations were along a two-mile line perpendicular to the expected mean flow. The fourth station was six miles upstream of the other three. Of the eight current measuring meters which operated successfully, three were at depths of approximately 15 m, two at 65 m and one each at 106 m and 218 m.

The currents were found to be rotary in a clockwise direction. A comparison with theory showed that the near-surface currents were of an inertial nature; the measured periods of the near-surface currents being almost equal to the theoretical inertial period of 15.5 hrs. A curve was constructed showing the form of the correlation between the rotary currents at different depths at one of the stations. A vertical spiral effect similar to the Ekman spiral but rotating in time was interpreted from the shape of the curve.

A study of measured iceberg tracks showed that the loops sometimes made by icebergs could quite possibly be caused by inertial current effects. One particular track which included several loops was examined in detail. The period and radius of the looping motion were found to be in the ranges of the inertial period and radius of influence.

Geostrophic current profiles were constructed for a line near our research area. The oceanographic data used were obtained through the Canadian Oceanographic Data Centre and came originally from the International Ice Patrol. In the years 1961 to 1964 the oceanographic data were

obtained using nansen casts while from 1965 onward the data were obtained using a Bisset-Berman, Salinity/Temperature/Depth (STD) Environmental Profiling System. All data were measured at approximately the same time of year. There were order-of-magnitude consistencies from profile to profile. It was hypothesized that a significant inertial current could result from a geostrophic current if the driving force behind the geostrophic current disappeared.

CHAPTER 1

INTRODUCTION

In recent years, large areas off the East Coast of Canada have been leased to petroleum companies for exploration. One of the big problems that will be encountered by this industry, especially in the Labrador Sea, is the presence of icebergs. These icebergs drifting in the Labrador Current represent a serious danger to drilling rigs. Little is yet known about iceberg drift, and before safe exploration and production activities can be assured, detailed knowledge of the phenomena is required. For this purpose, direct current measurements are essential. Up until now, very few such measurements have been made in the Labrador Current. Most existing information on the Labrador Current has been derived indirectly from measurements of salinity, temperature and depth data obtained by the U.S. Coast Guard International Ice Patrol. There have been several projects in the past three years in which direct current measurements were made. The U.S.C.G. International Ice Patrol tried out a mooring system in which there were two arrays of current meters, and the petroleum companies AMOCO and Mobile also made separate direct measurements. The data from all of these measurements are being processed and it is hoped that the results will be made available to the public in the near future.

From observations of iceberg motion, it is seen that there may be a main drift which can be determined reasonably easily. However, in addition to this, there are movements from the main drift path which are

more difficult to describe or to predict. The investigation presented in this thesis may shed some light on the description or prediction of these perturbations.

The area selected for this research was approximately at Longitude $52^{o}30'$W and Latitude $50^{o}30'$N where the presence of icebergs is very significant for several months of the year. The current was studied at horizontal positions over a spatial length scale of several miles and at depths of approximately 15 m, 28 m, 65 m, 106 m and 218 m. The shapes of the current velocity versus time curves are discussed with consideration of the horizontal current structure both at sub-stations at the same level and at sub-stations at different levels along a vertical line. The results are then related to actual plots of iceberg drift in the Labrador Sea.

The data necessary to compute geostrophic currents in the Labrador Sea have been collected for many years from the initiation of the International Ice Patrol. These are indirect current determinations using salinities, temperatures and depths measured at stations which are separated by horizontal distances of the order of 20 or 30 miles. The current patterns thus obtained are general ones and cannot usually be considered reliable in areas of spatial length scales of just several miles. As we have mentioned before, detailed knowledge of currents over small spatial length scales is necessary if a good understanding of iceberg drift is to be achieved. However, with all of the data available with which geostrophic currents may be computed, it may be worthwhile to ascertain if these current patterns, although of a general nature, may help to predict the occurrence of particular patterns in localized areas. If they are useful in this regard, the existing STD data measured in the Labrador Sea may gain more

importance relative to the needs of the offshore petroleum industry. In this investigation, a determination of the geostrophic currents through a line near the area of research was made, and an attempt was made to show a connection between these and the observed current field in our research area. The data used to determine the geostrophic currents were obtained at approximately the same time each summer for the years 1961, '62, '63, '64, '69 and '70. The data from 1961 to 1964 were obtained using nansen casts and from 1965 to 1970 using a Bisset-Berman Salinity/Temperature/ Depth (STD) indicating system. It was assumed that six years' data would be sufficient to show any consistencies in the current patterns.

CHAPTER 2

EXPERIMENTAL PROCEDURE

Descriptions of the apparatus and the experimental procedure are given here along with the method of data reduction.

2.1 Current Measuring Instrumentation

Ten Braincon type 316 Histogram Current Meters (H.C.M.), on loan from the Bedford Institute of Oceanography, were used to measure current. A complete description of the current meter and its specifications are given in the Appendix and are briefly summarized here. The current speed sensor used in the Braincon meter is a Savonius Rotor. It has a range of 0.05 to 5 knots, calibration threshold of 0.05 knot (minimum), minimum starting velocity of 0.01 knot, and a sensitivity of 83 R.P.M./knot. The sensor outputs are in concentric circular analog format and are recorded for a selected recording interval on successive frames of 16 mm film. The speed output has an accuracy of ± 3% of full scale (5.0 knots) when used with calibration curve and corrected for tilt. The current direction sensor is a large area vane (9.25 ft^2). It indicates magnetic direction from 0^0 to 360^0 (continuous), and its sensitivity is ± 5% at 0.05 knot. After development of the 16 mm film, the recorded data is reduced using a modified Eastman Kodak 310-PV Film Reader.

2.2 The Experimental Method

The placing of the current meters in the ocean was accomplished during a research cruise of the B.I.O. ship Dawson in June, 1971. Personnel

from B.I.O. handled the actual setting and recovering of the meters. Ten meters were placed, eight of which produced current data. The horizontal array had four stations as shown in Fig. 1. The stations A, B and C were selected to give transverse information on the current over a spatial scale of approximately two miles and station D was selected to provide longitudinal information over a scale of six or seven miles.

The vertical current meter array is shown in Fig. 2. Station A has four sub-stations (each meter position is equivalent to a sub-station), A1, A2, A3 and A4 at depths of 18 m, 28 m, 106 m and 218 m, respectively, with A4 about eight meters from the ocean bottom. This array at station A was designed to obtain the current structure at different water levels along a single vertical line. Sub-stations B2 and C2 at depths of 63 m and 65 m, respectively, were designed to test the spatial correlation at an intermediate depth. Sub-stations B1, C1, D1 and D2 at depths of 13 m, 15 m, 15 m and 17 m, respectively, along with A1 were near the surface in order to investigate the expected strong current structure there. The meters could not be placed closer to the surface than approximately 15 meters because of the adverse influences of surface disturbances.

The meter depths and the times over which the current meters were operational at each of the sub-stations are given in Table I. The total time column gives the recording times of the meters. The longest recording time was 75 hours 49 min. for A1. As the meters were set for 10-minute recording cycles, this time represents 455 individual current measurements with each measurement being a 10-minute average. The shortest recording time, 66 hours 44 min., for D1, represents 400 measurements. The current meters at sub-stations B1 and D2 failed to record properly and the data from these were discarded.

2.3 Data Reduction

The raw data on the 16 mm film was transferred to computer cards and sent to B.I.O. for processing. This process consisted of converting the raw data into current speeds and directions. The information was returned to us on magnetic tape containing eight files, one file for the data from each current meter. An IBM 370 computer was used to convert directions from magnetic to geographic north and then to obtain the components of the velocities along North-South and East-West lines. These components were separated into eight files, each representing the N-S components at each of the meter placements and eight files for the corresponding E-W components.

Spatial correlations between N-S components of current velocity at different sub-stations and between E-W components at the same corresponding sub-stations were computed. For this purpose, the data format was converted to a matrix form. The files representing the components in one direction were arranged so that each file became a column in the matrix. The columns were then shifted so that the current components in each row represented values measured at the same time. The correlation coefficients between files were obtained using a library Fortran program developed for Biomedical uses at UCLA in California, U.S.A. This program computes simple correlation coefficients, averages and measures of dispersion.

There are six main steps performed by the program for each X_{ij} value which is included in the computations. (X represents the current component in a given direction, and the subscripts i and j represent, respectively, the sample indicator number at a given time and the number of the file.) For example, the 3rd value in column 2 would be represented by $X_{3,2}$. The output from these steps includes sums, means, cross-product

deviations, standard deviations, the variance-covariance matrix and the correlation matrix. Optional output includes one-page cross-tabulation plots of any two variables.

The correlation matrix is given by

$$\frac{\Sigma(X_{ij} - \overline{X}_j)(X_{ik} - \overline{X}_k)}{\sqrt{\Sigma(X_{ij} - \overline{X}_j)^2 \, \Sigma(X_{ik} - \overline{X}_k)^2}}$$

where $\overline{X}_j$ is the mean of the j variable. The correlation matrix used in this form can be easily used to obtain time correlations, in a single file or between files, as well as obtaining the spatial correlations which were of interest to us.

CHAPTER 3

EXPERIMENTAL RESULTS AND DISCUSSION

The data obtained from the current meters are presented here as current velocity versus time curves along north-south and east-west lines. These curves are discussed with respect to theoretical considerations as well as iceberg drift. Current velocity vectors at sub-station A1 are plotted and spatial correlations are presented.

3.1 Current-Velocity versus Time Curves for the Near-Surface Sub-Stations

The curves of current components in the N-S and E-W directions versus time for the sub-stations A1, C1 and D1 are shown in Figs. 3, 4 and 5, respectively. The depths and positions of the stations are shown in Table I. The distance between the A and C stations is 2.1 mi. and the distance between the C and D stations is 6.5 mi.

The most noticeable factor in all of the figures is the almost sinusoidal nature of the curves. This factor is evident in both the N-S and E-W components. Also, the amplitudes of the curves for the three sub-stations are all approximately the same. The curves are nearly symmetrical about the zero velocity axis which indicates that there was very little translatory current.

In Table II, the average periods of the sinusoids are presented for the N-S and E-W curves at each sub-station and also the average period of the two components combined. The average lags between north and east maxima and between south and west maxima are included in the table as well as lag-period ratios and the ratios of average N-S amplitudes to average E-W amplitudes.

As shown in Table II, the periods of the sinusoids at the sub-stations A1, C1 and D1 were 15.3 hrs, 15.8 hrs and 15.2 hrs, respectively. The average lag to period ratios and the N-S amplitude to E-W amplitude ratios were almost the same at the three sub-stations.

These results strongly indicate that there was a rotary-type current in the experimental area during the time the current meters were operating. Moreover, it appears that, as the N-S amplitudes were not noticeably different from the E-W amplitudes and as the lags were nearly a quarter of the periods, the current was almost circular. The direction of the current determined from the positions of the current maxima is clockwise. We can obtain some idea of the degree of departure from a circular form by considering the deviations of the lag to period ratios from 0.25 which would be the ratio for a circular current. For the sub-stations A1 and D1, the ratios were 12% less than 0.25 and for sub-station C1 the ratio was 16% less than 0.25. This means that the form of the current was slightly elliptical with major axis approximately in a NW-SE direction.

This is a generalized conclusion, of course. The form of the current may have deviated more or less from the circular form than we have indicated over the entire time that the current meters were operating. Also, if the rotary current were superimposed on a translational current, the cumulative effect would be a cyloidal-type motion. For example, the current motion at sub-station A1 may have been of cyloidal nature in part as will be shown later in section 3. It may be noted, as well, that the amplitude of the current is about the same, $\sim$ 0.25 - 0.30 knot, at each sub-station as seen in Figs. 3, 4 and 5. This, along with the similarity of the form of the velocity-time curves, indicates that the same conditions

were obtaining in the ocean over a spatial scale of at least seven miles, i.e. the distance between stations A and D.

A similar phenomenon was reported by the International Ice Patrol (1950) at a location $45^{0}27'N$, $47^{0}57'W$, i.e. several hundred miles further south of the position of our area of research. A rotary-type current was observed which had a period of about 16 hours which is very close to our values of 15.3 hrs, 15.8 hrs and 15.2 hrs at sub-stations A1, C1 and D1, respectively. However, the motion obtaining in the I.I.P. (1950) study had a distinct translatory component as well as the rotary component. As noted previously, the current in our research area did not contain a significant translatory component.

This rotary-type current measured by the I.I.P. was thought, at first, to have been of tidal origin. However, there was no tidal constituent suitably strong enough to maintain such a motion. Then, it was suggested that this could have been an inertial current, although this possibility was not explored theoretically or otherwise. It was felt by us that the latter suggestion was worthy of investigation in our case. After considering the theory of currents, it became apparent that the type of current we had measured was most likely of inertial nature. This inertial aspect is explored in the following section.

3.2 Theoretical Considerations

In order to arrive at the equations which describe the motion of inertial currents, use will be made of the hydrodynamic equations of motion as applied to a continuous volume of fluid on a rotating earth. They are, as given by Neumann (1968),

$$(3.1) \qquad \frac{du}{dt} = -\frac{1}{\rho}\frac{\partial P}{\partial x} + 2\omega \sin\phi \cdot v + F_x$$

$$(3.2) \qquad \frac{dv}{dt} = -\frac{1}{\rho}\frac{\partial P}{\partial y} - 2\omega \sin\phi \cdot u + F_y$$

and

$$(3.3) \qquad \frac{dw}{dt} = -\frac{1}{\rho}\frac{\partial P}{\partial z} + g - 2\omega \cos\phi \cdot u + F_z$$

where u is the horizontal velocity in the +ve x-direction (East)

v is the horizontal velocity in the +ve y-direction (North)

w is the velocity in the +ve z-direction (downward)

ρ is the density of the water

P is the pressure

ω is the angular velocity of the earth

ϕ is the latitude

g is the acceleration due to gravity

and F represents all frictional forces that may be acting on the fluid.

In the case of frictionless motion with dw/dt = 0 (non-accelerated currents), eq. (3.3) becomes

$$(3.4) \qquad \frac{\partial P}{\partial z} = g\rho \left(1 - \frac{2u\omega}{g}\cos\phi\right) .$$

It can be shown that under ordinary conditions in the ocean, the term $(2u\omega \cos\phi)/g$ can be neglected in eq. (3.4) and, hence, eq. (3.4) reduces to the hydrostatic equation $\partial P/\partial z = g\rho$.

If the two dimensional (horizontal) current field is also frictionless, then eqs. (3.1) and (3.2) take the form

$$(3.5) \qquad \frac{du}{dt} = -\frac{1}{\rho}\frac{\partial P}{\partial x} + 2\omega \sin\phi \cdot v$$

and

$$\frac{dv}{dt} = -\frac{1}{\rho}\frac{\partial P}{\partial y} - 2\,\omega \sin\phi \cdot u \quad . \tag{3.6}$$

The accelerations on the left-hand, including the Coriolis accelerations, are balanced by the forces per unit mass resulting from horizontal pressure gradients. These gradients may be caused, for example, by an inclination of the sea surface in a homogeneous ocean under the effect of a wind stress. If these gradients vanish, then

$$\frac{du}{dt} = 2\,\omega \sin\phi \cdot v \tag{3.7}$$

and

$$\frac{dv}{dt} = -2\,\omega \sin\phi \cdot u \quad . \tag{3.8}$$

The acceleration of any water particle balances the Coriolis acceleration, and a current with the velocity $c = \sqrt{u^2 + v^2}$ continues to flow by its own inertia. Such currents are called inertia currents.

From eq. (3.7) and (3.8), we have

$$u\frac{du}{dt} + v\frac{dv}{dt} = 0 \quad . \tag{3.9}$$

Because $\frac{d}{dt}(u^2 + v^2) = \frac{d}{dt}(c^2) = 2u\frac{du}{dt} + 2v\frac{dv}{dt}$, it is seen that eq. (3.9) states that $\frac{1}{2}\frac{d}{dt}(c^2) = 0$ which means that each water particle moves with constant speed. The acceleration of a water particle results from a change in the direction of motion.

It can be shown that

$$\frac{d\alpha}{dt} = -2\,\omega \sin\phi \tag{3.10}$$

where α denotes the angle between the x-axis and the direction of the current, c.

Therefore, the moving particle must move in a circle with constant speed. This circle is called "the circle of inertia". In the Northern Hemisphere ($\phi > 0$) $\frac{d\alpha}{dt} < 0$, and the motion is anticyclonic.

Letting r = radius of the inertia circle and T_p the period of the motion, then $T_p = 2\pi r/c$ and the Coriolis acceleration is balanced by the centrifugal acceleration c^2/r so that $c^2/r = 2\,\omega \sin\phi \cdot c$.

It follows that

$$r = \frac{c}{2\,\omega \sin\phi} \tag{3.11}$$

and

$$T_p = \frac{\pi}{\omega \sin\phi} \quad . \tag{3.12}$$

We now apply eq. (3.12) to our situation, that is, with $\phi = 50^{o}30'$. This gives a T_p of 15.5 hours which agrees extremely well with the periods found in our study. As our velocity-time curves were symmetrical about the zero velocity axis, there was little translatory motion. It may be concluded that the currents obtaining in the area were mainly rotary inertial currents.

This leads us to consider the importance of r in eq. (3.11). For the currents in our research area, c was approximately 0.25 knot. Substituting this value in eq. (3.11), we obtain for r a value of 0.62 naut. mile. Because of the complexity inherent in inertial currents regarding particle motion, we would prefer to refer to r as a "scale of influence" rather than a radius. We will investigate later how significant this "scale of influence" is in the drift of icebergs.

3.3 Current-Velocity versus Time Curves for Sub-Stations along a Vertical Line

The current-velocity versus time curves of the N-S and E-W components for the A sub-stations are given in Figs. 6, 7, 8 and 9. The A1 sub-station curves are reproduced here to facilitate convenient comparison with the nature of the current at the other A sub-stations which are vertically below A1. The depths for the sub-stations A1, A2, A3 and A4 as given in Table I are 18 m, 28 m, 106 m, and 218 m, respectively.

It is apparent that the sinusoidal effect is evident at all sub-stations. Again, the curves are symmetrical about the zero-velocity line indicating a zero translatory current. The average periods of the N-S and E-W components and the combined average periods are given in Table III. Also presented in the table are average lags between north and east maxima and between south and west maxima, average lag to period ratios, and the ratios of average N-S current amplitudes to average E-W current amplitudes.

The average lag to average period ratios for the sub-stations A1, A2, A3 and A4 are 0.22, 0.25, 0.21 and 0.15, respectively. The ratios of the current amplitudes of the N-S and E-W components are very nearly unity. With a lag to period ratio of 0.25, equal N-S, E-W current amplitudes and zero translatory current, the motion would be circular. Hence, the current remained rotary and only slightly elliptical down to the 106 m depth of A3. The A4 sub-station was at a depth of 218 m and was only eight meters from the ocean floor. Although the current was still somewhat rotary there, as seen in Fig. 9, the lag to period ratio of 0.15 indicates much greater ellipticity in the current form than in the current forms at sub-stations A1, A2 and A3. It is very probable that the bottom topography influenced

the structure of the current at the A4 sub-station effecting the departure from a circular form.

The periods of the motions at the sub-stations A1 and A2 are approximately the same, 15.3 hrs and 15.4 hrs, respectively, which are in good agreement with the theoretical value of 15.5 hrs determined previously for a rotary inertial current at latitude $50^{\circ}30'$. At greater depths, i.e. 106 m and 218 m, we find that there is a decrease in the period to 13.4 hrs and 12.0 hrs, respectively. From Figs. 6, 7, 8 and 9, it can be seen that the amplitudes of the motions decrease from $\sim$ 0.25 knot at A1 to $\sim$ 0.10 knot at A4. We can consider these values with respect to our previous conclusion that the rotary currents which were measured were very likely inertial.

As an inertial current is generally the result of a current which was produced mainly by near surface effects, it is reasonable to assume that, because of friction, the current velocity would decrease from the surface to the bottom. If indeed the current were inertial, the decrease in period may be explained in the following manner. The inertial current was initiated and therefore very dominant in the upper levels of the ocean. Due to frictional coupling, the effect of the inertial current was evident at neighbouring lower levels. Although the current amplitudes would be less at these levels than at the upper levels, the periods of the motions are the same. Our decrease in period from 15.4 hrs at the 28 m level to 13.4 hrs at the 106 m level indicates that, at some depth between 28 m and 106 m, the rotary inertial current had ceased to be the dominant factor and that some other factor increased in importance.

The 12.0 hr period at the 218 m level could mean that this other factor was of tidal origin. The 13.4 hr period at the 106 m level could

then possibly be explained as the effect of coupling between the inertial and tidal currents. The main problem with this tidal explanation is that there was no evidence of a 12.0 hr component at the 18 m and 28 m depths. Another suggestion has been made that maybe the stratification of density would effect a change in period of the inertial current with an increase in depth. However, the effect, if any, of an increase in density would be an increase in the period rather than a decrease. The author has also considered the possibility that an increase in viscosity with depth would cause a decrease in the period of the inertial current. This possibility was ruled invalid as the period was found to be independent of frictional forces. It is planned to look into this problem in more detail in a "post-thesis" study.

3.4 Current Velocity at Sub-Station A1

An interesting way to investigate the current motion is presented in Fig. 10 which is a plot of the current vectors at sub-station A1 for the three-day period from 12:00 NDT June 6, 1971, to 12:00 NDT June 9, 1971. For convenience, the plot was made in separate 24-hr sections. Each point represents the tip of a velocity vector with its beginning at the origin of the co-ordinate system. The time interval between successive points is one hour.

The rotary nature of the current is apparent as expected. There is a slight displacement toward the SW giving a small translational motion in that direction. The average magnitude of the vectors is 0.25 knot. The average centripetal acceleration determined from $\Delta\vec{v}/\Delta t = 2\pi v/T$, where $\vec{v}$ is the velocity, t is the time and T is the period (= 15.3 hrs), is 0.10 mile/hr^2 which gives, when equated with v^2/r, a radius of influence r of 0.61 mile.

Another method of displaying the current velocity vectors is shown in Fig. 11 for the case of sub-station A1. The vectors are added successively to achieve a cumulative vector diagram. The range of influence r (= d/2) is 0.50 mile for the well-defined loops and spiral. The average velocity vector $\vec{v}$ taken to the 64th hour after the beginning of measurement is 0.056 knot SW. This value is approximately 20% of the average magnitude of the velocity vector. A similar plot for sub-station A2 gave similar results, with the translational component being approximately 20% of the average velocity and also in the SW direction. For sub-station A3, the translational component was only 13% of the average velocity and in the NW direction.

Sverdrup et al (1942) have suggested that such a curve as shown in Fig. 11 represents the path taken by a water mass if it is assumed that the observed motion is characteristic of a considerably extended water mass. If indeed this suggestion is valid, then the curve in Fig. 11 could also represent the path of an object moving with the current provided the physical dimensions of the object were small in comparison to the scale of influence of the current and provided the mass of the object was not so great that its inertia would keep it from changing direction with the current. We will see later in section 3.6 that there are some similarities between the type of motion possibly represented by Fig. 11 and the motions of several iceberge observed in the Labrador Sea by Dempster and Bruneau (1972).

3.5 Spatial Correlations

When this research idea was conceived, it was expected that we would find strong translatory currents in the experimental area. The

little detailed information that was available about currents in the area led us to believe that this would be the case. The spatial correlations between sub-stations, presented in Table IV, were mainly intended to investigate the scales of disturbances, if any, associated with the translatory flow. Although, in this respect, the relevance of these correlations has decreased in view of the nature of the currents that were actually obtaining, they may help us to interpret our results more completely.

In Table IV, the spatial correlations between N-S current components and between E-W current components at pairs of sub-stations are given. The depths of the sub-stations are also included. The top group of correlations is for pairs of sub-stations which are separated vertically from each other. The bottom group is for pairs of sub-stations which are separated horizontally or almost horizontally.

There are high correlations in general in the bottom group between sub-stations separated horizontally. One would expect this if the current meters were in a large water mass moving approximately in a circle in such a way that all parts of the mass followed approximate circular paths of equal radii and had constant magnitude of velocity at all times. That is, the water mass would be moving as a solid mass without rotation about its centre. The correlation of 0.86 for both the E-W and N-S current components between sub-stations A1 and C1 is very high and indicates that the water mass remained irrotational over the spatial scale of at least two miles, i.e. the separation between A1 and C1.

In Fig. 12, we have plotted the correlation coefficients between the pairs of sub-stations A1-A2, C1-C2, A2-A3, A1-A3 and A1-A4 as a function

of the difference in depth between each sub-station pair. The curve is drawn taking into account both the N-S and E-W correlation coefficients. Although it would have been preferable to have used only correlations between pairs along one vertical line, it was felt that the C1-C2 correlations could be used here in view of the great similarity between the current at sub-stations A1 and C1.

The N-S and E-W current components as functions of time were nearly sinusoidal, so we would expect the form of the correlations curve in Fig. 12 to be similar to one which would be obtained if they were sinusoidal.

To interpret the form of the curve, we first consider the correlation between two sine curves of equal frequency but with a phase lag. Assume that the sine waves are functions of time and have constant amplitudes. For a phase lag of zero, the correlation coefficient is +1. As the lag increases, the correlation decreases, passing through zero when the lag is $\pi/2$ and reaching -1 when the lag is π. With further increase in the lag, the correlation increases to zero when the lag is $3\pi/2$ and +1 again when the lag is 2π. We next consider the correlation between two sine waves as a function of frequency difference. At zero frequency difference, the correlation coefficient is +1. As the difference increases, the correlation decreases until it reaches a minimum at a negative value whose magnitude is less than unity. With further increase in the frequency difference, the correlation increases until it reaches a maximum at a positive value less than +1 and so on, the value of each successive maximum being less than the previous value.

Initially, the curve in Fig. 12 decreases with an increase in depth until it reaches a minimum at a depth difference of 95 meters where

the correlation coefficient is -0.45. There is then an increase to what appears to be a small positive maximum at 200 meters depth difference. The form of the curve agrees well with the previously discussed form for the correlation between two sine waves as a function of frequency difference. For the sub-stations A1, A2, A3 and A4, the frequencies of oscillation were 0.065 hr^{-1}, 0.065 hr^{-1}, 0.075 hr^{-1} and 0.083 hr^{-1}, respectively. The difference in frequency between A1 and A4 is not large enough to fully explain the form of the curve. Another important factor is the lags, caused by friction, between the current at different levels. Assuming that the motion of the large scale water mass was near-surface generated, the lag between the surface current and currents at lower levels increases with depth difference. The form of the curve in Fig. 12 is similar to the form for the correlation between two sine waves of equal frequency whose phase difference steadily increases.

We conclude that there were both frequency and phase differences between the rotary currents at different levels. These differences increased with an increase in vertical separation of the currents. At a given time, the current direction at different levels along a vertical line from the surface to the bottom must have changed always in the same sense. The current magnitude decreased with depth. Hence, at a given time, a curve through the tips of the velocity vectors along a vertical line would describe a spiral.

The spiral for rotating currents may be compared to the Ekman spiral for wind-driven currents. The Ekman spiral is mainly the result of friction, between adjoining levels, arising from vertical shearing stresses. The rotary current spiral is due to frequency differences as well as vertical shearing stresses. Unlike the direction of the wind-driven

current, the direction of the rotary current is not constant at a particular point. The Ekman spiral, after equilibrium conditions have been reached, is approximately stationary in space and time, whereas the spiral for the rotary currents continuously rotates. The difference between the two types of spirals can be primarily attributed to the presence of the time differentials du/dt and dv/dt in the equations of motion for the rotary currents and the absence of these differentials in the equations of motion for wind-driven currents.

The correlation coefficients plotted in Fig. 12 were obtained from data accumulated over a three-day period. These coefficients were sufficient to provide a general form for the correlation curve. Longer total measurement times in comparison to the periods of the motions would be necessary if more detailed correlation information is needed.

3.6 Some Aspects of Iceberg Drift

The possibility is now explored of a connection between the nature of the current in our study and the actual drift of icebergs. The report of Dempster and Bruneau (1972) discusses an extensive study of iceberg drift in the Labrador Sea off the coast of Labrador. More than one hundred icebergs were tracked for periods extending from a few hours to several days. Several of the tracks are reproduced here in Fig. 13. Deviations from smooth streamline flows are evident in the drift patterns with some bergs exhibiting looping and spiraling. It was shown by the authors that there was a tidal influence (that of the principal lunary semi-diurnal component of period 12 hours and 25 minutes) in the inshore tracks. Because of the strong translatory currents inshore, the tidal influence appeared as small periodic indentations. An example of this is

the path of 12C in Fig. 13. The looping and spiraling evident in the offshore tracks 10F, 7M, 13G, 11S and 11L were not shown explicitly by Dempster and Bruneau to be due to tidal influence. In view of the similarity between several portions of these tracks and the 'virtual displacement diagram' of Fig. 11, we decided to examine in detail the motion represented by track 10F to try to ascertain if the looping was influenced by rotary inertial currents.

The N-S and E-W velocity components are plotted against time in Fig. 14 for the iceberg whose motion is represented by track 10F. Because of the loops made by this iceberg, it would appear that the oscillations were of a periodic nature. In order to verify this, sinusoidal curves with 12-hour periods were drawn symmetrically about the average translational velocity. The comparison between the experimental points and the sinusoidal curve is inconclusive.

To explore the idea that the iceberg may have been moving in an inertial current, the points in Fig. 14 are replotted in Fig. 15 over sinusoidal curves with a 16-hour period. Again, the comparison between the experimental points and the curves in inconclusive. Other sinusoidal curves with periods of 14 hours and 15 hours were also compared with the experimental data but with no result.

Unfortunately, the displacement data for the track 10F are not complete enough to allow an accurate determination of the radii of the

loops. A rough value of the radii, obtained from a displacement plot, is one mile. The "radius of influence" of inertial motion at the latitude of the iceberg is approximately 0.7 mile. This is of the same order as the rough value of the radii of the loops, but we hesitate to draw any concrete conclusions from the comparison. Little is known about the motion of icebergs under the influence of a rotary current, and the relationship between the current and the icebergs' motion has not yet been established.

The possibility of inertial influence in the drift of icebergs is examined further by considering some tracks obtained under ocean conditions different from the conditions prevalent when the tracks of Fig. 13 were obtained. After an atmospheric low pressure had moved over the experimental area of Dempster and Bruneau (1972), the tracks of the icebergs changed character appreciably as shown in Fig. 16. It appears that slope currents were established while the pressure disturbance was moving over the area. This caused patterns of drift which were more irregular than those previously obtained. The icebergs seemed to execute more loops and spirals than before the pressure disturbance occurred. It is possible that, in certain areas of the experimental region, the slope currents became rotary inertial currents after the driving forces had vanished, and that, in some cases, these inertial currents were dominant with the motion having little translation.

CHAPTER 4

GEOSTROPHIC CURRENTS

It was mentioned in the introduction to the thesis that much oceanographic data have been measured in the Labrador Sea from which geostrophic currents may be computed. These currents are considered to represent average current magnitudes rather than the almost instantaneous values found by direct measurement. This is because the oceanographic conditions are assumed not to change appreciably in short periods of time. A significant change would probably occur in several days rather than several minutes. Also, the measurements of salinity, temperature and depth have usually been made at stations separated from each other by distances of the order of 20 or 30 miles. Hence, the geostrophic current patterns obtained are general not only with respect to time but also spatially.

Even though it appears that the use of such patterns would not be applicable in localized areas, it was considered worthwhile to explore the possibility that they could help to predict local patterns. Toward this end, some geostrophic current profiles were determined from data acquired near our experimental area. The data were measured each year in late July in the years 1961, '62, '63, '64, '69 and '70. The profiles were studied to ascertain if there were consistencies in the current patterns from year to year. Some aspects of these geostrophic current patterns were then compared with the current pattern obtaining at the time of our research.

4.1 A Brief Outline of the Theory of the Dynamic Method of Computing Geostrophic Currents

According to Defant (1961), "The scientific treatment of observational data cannot be considered complete if it does not include dynamic methods." The dynamic method in oceanography is one which does not take into account frictional forces. It considers the equilibrium between the Coriolis force and the force due to the horizontal pressure gradient. The method thereby excludes the effect of the wind as a driving force, and also it assumes that the currents are not accelerated.

A brief summary of the basic theory of geostrophic currents is given here. Beginning by equating the components of the Coriolis force and the pressure gradient force along each horizontal co-ordinate direction (x is positive facing east, y is positive facing north), the Navier-Stokes equation in cartesian co-ordinates simplifies to

$$2\omega \sin\phi \cdot \rho v = \frac{\partial p}{\partial x} \tag{4.1}$$

and

$$2\omega \sin\phi \cdot \rho u = -\frac{\partial p}{\partial y} \tag{4.2}$$

with the usual notation.

It is assumed that the component of the Coriolis force along the vertical (z) direction is negligible here and that the hydrostatic equilibrium can be approximated by the hydrostatic equation $\partial p = g\rho\partial z$ where g is the acceleration due to gravity and z is positive downwards.

Squaring equations (4.1) and (4.2), adding and taking the square root, we obtain

$$2\omega \sin\phi \cdot \rho c = \frac{\partial p}{\partial n} \tag{4.3}$$

where $c = (v^2 + u^2)^{\frac{1}{2}}$ is the geostrophic current and $\frac{\partial p}{\partial n} = \left[\left(\frac{\partial p}{\partial x}\right)^2 + \left(\frac{\partial p}{\partial y}\right)^2\right]^{\frac{1}{2}}$.

If we consider two oceanographic stations A and B, the dynamic depth differences (D_A and D_B) of two isobaric surfaces between the stations can be determined from

$$D_A - D_B = \int_{P_1}^{P_2} \delta_A dp - \int_{P_1}^{P_2} \delta_B dp \tag{4.4}$$

where δ is the anomaly of the specific volume of sea water.

It can be shown that

$$\frac{\partial p}{\partial n} = - 10\, \rho\, \frac{\partial D}{\partial n} \quad . \tag{4.5}$$

Hence,

$$2\, \omega \sin \phi \cdot c = - 10\, \frac{\partial p}{\partial n} = - \frac{10(D_B - D_A)}{\Delta n}$$

where Δn is the horizontal distance when proceeding from station A to station B.

Therefore,

$$c = - \frac{10(D_B - D_A)}{2\, \omega \sin \phi \cdot \Delta n} \quad . \tag{4.6}$$

Here, c is relative velocity between two isobaric surfaces. It can be shown, Neumann (1968), using the hydrostatic equation that there is a certain depth at which $\frac{\partial p}{\partial n} = 0$ and, hence, the absolute geostrophic current should also be zero at this depth. If this "layer of no motion" is known, a zero reference level is provided to convert relative velocities into absolute velocities.

4.2 Determination of the Zero Reference Level

There are many different methods available to estimate the topography of the zero reference level. The one presented by Defant (1961)

appears to be the most practical to use here because it can be applied to areas in which the bottom depth is fairly shallow as is the situation in this study. Defant's method is as follows.

The differences in dynamic depth between two neighbouring stations are plotted against depth. In most cases, this difference becomes approximately constant through a layer of considerable vertical thickness. This layer then is either moving with constant velocity or is motionless or almost motionless. From probability considerations alone, one may deduce that the latter explanation is the more plausible. The zero reference level should, therefore, lie within this layer. The calculated current velocity in this layer is then subtracted from the velocity values at other depths in order to determine the absolute velocities at those depths.

Fomin (1964) questions the validity of this method in shallow waters. He criticized the work of Neumann (1942) who determined the "zero" surface in the Black Sea using Defant's method and then computed the geostrophic currents at the surface. Fomin contended that the method should perhaps not be used in areas where the bottom could have an effect on the straightening of the dynamic depth curves. However, Neumann's results agreed with the observational data of currents in the Black Sea. We conclude that, although Fomin's criticism may be academically justifiable, until a more satisfactory solution to the problem is formulated, one must be practical and use the method which produces the most reliable results.

4.3 Calculations

The raw data for this study were supplied to us by the Canadian Oceanographic Data Centre. The calculation of the relative geostrophic currents was a direct application of equation (4.6). The current patterns

through the section shown in Fig. 17 were obtained for the years 1961, '62, '63, '64, '69 and '70. The station numbers in the original data report were changed to begin at 1 on the right and end at 8 on the left of the section. The station numbers and latitudes and longitudes of the stations are given in Table V.

The zero reference levels were determined by plotting $(D_B - D_A)$ against depth as shown in Figs. 18-23. In most cases, the reference layer was well defined and no serious problems arose. For the cases where the plot did not straighten appreciably, the bottom was taken as the reference.

The values of the dynamic depth differences were fed into a computer program along with other essential data and the values of the relative velocities were calculated using equation (4.6). An example of the computer print-out of the results is shown as Table VI. In this table, the depth and distance between successive stations (DISTANCE) are given in meters. The successive stations are designated by their latitudes (LATITA, LATITB). The velocity values are given in meters per second. The relative velocities are under the heading REL VEL. The absolute velocities (ABS VEL) were determined by subtracting the appropriate values of the zero reference level velocities from the relative values.

The method which was used to construct the velocity profiles is similar to the one presented in the report of the Marion and General Greene Expeditions (1928). For each year, the absolute velocities were plotted as mean values between successive stations. An example of one such plot is Fig. 24 which is for the year 1962. At the depths 0, 10, 50, 100, 200 and 300 meters, the mean velocity lines were drawn. Then a continuous curve representing the velocity was constructed at each depth such that between

adjacent stations, equal areas are formed on either side of the previously fixed lines of mean velocity, and the curves are flattest near the margin and near the axis of each band. To complete the construction of the velocity profile, the curves for all the levels were projected on to their respective depths in a vertical plane and equal values of the same sign were connected.

The resulting velocity profiles for the years 1961, '62, '63, '64, '69 and '70 are shown in Figs. 25-30, respectively. The variation in the bottom topography from figure to figure is due to the fact that the station positions were not precisely the same each year. The solid contours mean that the current is moving through the section perpendicularly from right to left as one looks from station 1 towards station 8. This direction is approximately SSE and shall be denoted +ve. The dashed contours signify the opposite direction (NNW) which shall be denoted -ve.

It is evident that there are no strong yearly patterns. However, there are general consistencies. The solid contours centered around station 5 in Fig. 26, those between stations 6 and 7 in Fig. 27, those between stations 7 and 8 in Figs. 28, 29 and 30, and those centered around station 6 in Fig. 31 are all similar in maximum magnitude (approx. 30 cm/sec) and shape. As one would expect, the flow in the -ve direction was not, in general, appreciable, there being only one year, 1964 (between stations 2 and 3), which exhibited a strong -ve current. There were indications in other years of negative currents though of much smaller magnitudes than that obtaining in 1964. As the oceanographic data were collected each year in late July, the velocity profiles fit the general pattern one would expect for that time of year.

4.4 Discussion with Respect to Results of Chapter 3

Except for the currents obtaining in 1964, the maximum magnitude of the geostrophic currents at the surface is, in general, around 20 cm/sec (i.e. 0.40 knot). At the 200-meter level, the magnitude is of the order of 5 cm/sec (i.e. $\sim$ 0.10 knot). From our current meter measurements, the magnitude at the surface was of the order of 0.30 knot and at the 200 meter level it was of the order of 0.10 knot. Hence, the current magnitudes agree favourably between the calculated geostrophic and the observed currents.

It may be of interest to hypothesize that the observed inertial current originated from a translational current of a geostrophic nature. This could be the case if the driving force which caused the translational flow disappeared. The driving force is caused mainly by horizontal pressure gradients plus, in the case of slope currents, vertical shearing stresses. Because of the influence of friction in the motion of slope currents, these are not geostrophic but may be considered approximately geostrophic if the vertical shearing stresses are small. The horizontal pressure gradient due to salinity and temperature differences could be offset by a horizontal pressure gradient of opposite sign established by a sloping sea surface after the first gradient had instigated translational flow. This would mean the disappearance of the driving force, and consequently, the flow would become inertial.

It is also possible that changes in salinity and temperatures could occur in such a way as to bring about a zero horizontal pressure gradient after a translational flow had been established; creating an inertial current. The frequency of occurrence of such inertial currents could be determined from the probability of occurrence of zero horizontal pressure gradients closely following significant horizontal pressure

gradients in the same area. We can see from the current profiles presented in Figs. 22-27 that zero velocities (indicating zero horizontal pressure gradients) and fairly high velocities (indicating significant horizontal pressure gradients) are not uncommon. To determine how long it would take for a strong pressure difference to decrease to zero in a particular area would require successive STD measurements at the same stations over a time sufficiently long enough to cover the complete change of pressure. The geostrophic current profiles for each of the measurement times could be constructed. The time for velocity changes in a particular area would give the times for the corresponding horizontal pressure changes. Also, a rough estimate could be made of the 'width' of a particular geostrophic current from the profiles. If this current were to become an inertial current, the 'width' would provide a rough spatial scale for the inertial influence. For example, we have already seen that the phenomena observed in our experimental area had a spatial scale of at least seven miles. The scale may have been much larger, probably about 20 or 30 miles, which, as can be seen in Figs. 25-30, is of the same order as the 'widths' of the stronger geostrophic currents.

It would appear in theory, then, that there is some possibility that an inertial current can originate from a current of a geostrophic nature. However, no conclusive evidence of this can be discerned from our results. We have offered suggestions on how geostrophic current profiles may be used in helping to predice the occurrence of inertial currents in an area. Because of the generality of the profiles, it is unlikely that accurate predictions could be made from them even if profiles were available for an area representing currents at successive times of short separation.

CONCLUSIONS

This research has shown that current measurements and their analysis may play an important role in the determination of the basic reasons why icebergs behave as they do. Combining these reasons with the appropriate statistical data, it may then be possible to deduce probability patterns of iceberg motion in localized areas. Although our research has explored only one particular aspect (i.e. measured rotary inertial currents), there are other factors, above all, tidal, which initiate perturbations from smooth streamline flow. Current measurements would also be valuable in analyzing the effects of these factors.

The geostrophic currents in our study were indirectly derived from standard oceanographic measurements taken at stations which were far apart. We would suggest a more comprehensive study of geostrophic currents in a compact area. Such a study made under the proper conditions may show that detailed geostrophic current patterns would be useful in predicting the occurrence of rotary inertial currents in a particular area.

APPENDIX

The following specifications for the Histogram 316 current meter have been taken from the Instruction Bulletin issued by Braincon, Corp.

CURRENT SPEED SENSOR

TYPE: Savonius Rotor (Balanced in Air)
SPEED RANGE: 0.05 to 5 Knots
CALIBRATION THRESHOLD: 0.05 Knots (Minimum)
MINIMUM STARTING VELOCITY: 0.01 Knots
SENSITIVITY: 83 R.P.M./Knot
MOUNTING: Tungsten Carbide Pivot Bearings to Instrument Pressure Case

CURRENT SPEED OUTPUT

FORMAT: Circular Analog
SENSITIVITY: 78.85°/Knot for 20 Min. Recording Cycle (19 Min. Record)
INDICATOR: Radioactivated Phosphorescent Light Source (Half Life 1500 years)
TRANSFER MECHANISM: Magnetically Coupled Precision Gear Train (7200:1 Maximum Reduction)
ACCURACY: ±3% of Full Scale (5.0 Knots) when used with calibration curve and corrected for Tilt when required, including Total Error Band.

CURRENT DIRECTION SENSOR

TYPE: Large Area Vane (9.25 Ft.^{2} – Balanced in Water to be insensitive to Tilt)
MAGNETIC DIRECTION: 0 to 360° (Continuous)
SENSITIVITY: ±5° at 0.05 Knots
MOUNTING: Faired Fiberglas Clamp Locked to Instrument Pressure Case.
BEARING MATERIALS: Teflon and #316 Stainless Steel

CURRENT DIRECTION OUTPUT

FORMAT: Circular Analog – Viscous Jamped Permanent Magnet Compass
SENSITIVITY: ±0.5°
INDICATOR: Radioactivated Phosphorescent Light Source (Half Life 1500 years.)
TRANSFER MECHANISM: Direct Through Instrument Pressure Case
ACCURACY: ±1° (±0.3% Full Scale)

INSTRUMENT TILT AND DIRECTION SENSOR

TYPE: Inverted Plumbob – Viscous Damped
TILT RANGE: 0° to 40°
DIRECTION: 0° to 360° (Continuous)

INSTRUMENT TILT AND DIRECTION OUTPUT

FORMAT: Circular Analog – Viscous Damped
SENSITIVITY: ±0.5° Tilt, ±0.5° Direction
INDICATOR: Radioactivated Phosphorescent Light Source (Half Life 1500 Years)
TRANSFER MECHANISM: Direct
ACCURACY: ±1.0° Tilt Angle, ±1.0° Tilt Direction

RECORDER

METHOD: Direct Photographic Time Exposure of Sensor Outputs
CAMERA: Demountable, Motor Driven Film Transport
FILM TYPE: 16 mm Movie Film (Double-X Negative) 100 Ft. Spool, Kodak S-90
LENS: 6.5 mm – f 1.9 (Elitar)
POWER: One Eveready No. 744, 6 Volt Dry Cell

MODE

NUMBER OF RECORDINGS: 3600
RATE: 1 Frame/5 Min. to 1 Frame/Hour
MAX. UNATTENDED RECORDING PERIOD: 5 Months at 1 Frame/Hour
TEST: Continuous, 1 Frame/Min.

TIMING MECHANISM

TYPE: Solenoid Wound, Spring Driven, Jeweled Lever Clock – Shock Mounted
ACCURACY: ±10 seconds/day, Rate Adjusted
POWER: Uses same No. 744, 6 Volt Dry Cell as Camera with a 4.7 ohms dropping resistor

OPERATING ENVIRONMENT

INSTRUMENT STARTING MECHANISM: Mercury Switch, Vertically Oriented
OPERATING MEDIUM: Sea Water
OPERATING TEMPERATURE RANGE: 28°F to 90°F (–2°C to 65°C)
STORAGE TEMPERATURE RANGE: –30°F to 149°F (–34°C to 65°C)
***MAXIMUM PRESSURE:** To 10,000 psi (External)
SHOCK: Will withstand 6" drop to wood surface
MAXIMUM TENSILE LOAD: 8000 lbs. across Instrument Suspension Bar
***MAXIMUM OPERATING DEPTH:** To 6000 Meters

INSTRUMENT HOUSING

***MATERIAL:** Aluminum (6061-T6 or 7075-T6 Fed. Spec. QQ-A-200 or equivalent)
FINISH: Anodized to MIL-A-8625a (Type 2) Black
COATING: Double Coated with Synthetic "H" Coating
COLOR: Black (Other Coating and Colors Available)
HARDWARE: 18-8 Stainless Steel Welded Where Necessary
ANTI-CORROSION PROTECTION: Sacrificial Magnesium Anode
ANTI-FOULING PROTECTION: Applied Commercial Coating to Sensors if required
CONDENSATION CONTROL: Replaceable Desiccant
MAXIMUM LENGTH: 46⅜" Between Top and Bottom Mooring Eyes
MAXIMUM INSTRUMENT O.D.: 8½"
MAXIMUM WIDTH, INCLUDING DIRECTION VANE: 45⅛"
MAXIMUM WEIGHT IN AIR: 95 lbs,. approx. (½" Wall Tube and 1½" End Caps)
MAXIMUM WEIGHT IN SEA WATER: 67 lbs. approx.

*Subject to customer requirements.

ACKNOWLEDGMENTS

The author wishes to express his sincere thanks to Dr. R. T. Dempster who supervised the research work presented in this thesis. Especially appreciated are the stimulating discussions about the research.

Grateful acknowledgments are extended to the personnel of the Bedford Institute of Oceanography who helped in the reduction of the current meter data and to the crew of the Dawson who handled the setting of the current meters.

The assistance in this research of Dr. J. Allen is appreciated.

Thanks are also due to Neil Kennedy of NLCS who helped to prepare one of the computer programs, to Brian Gamberg who helped in the preparation of the diagrams, and to Miss Deanna Janes who typed the thesis.

REFERENCES

1. Biomedical Computer Program developed at UCLA, California, U.S.A. (available at NLCS, St. John's, Nfld.).
2. Canadian Oceanographic Data Centre, Ottawa, Canada (private correspondence).
3. Defant, A. 1961. Physical Oceanography, Vol. I, The MacMillan Co.
4. Dempster, R. T. and Bruneau, A. A. 1972. Project Report. "Dangers Presented by Icebergs and Protection Against Them." Memorial University of Newfoundland.
5. Fromin, L. M. 1964. The Dynamic Method in Oceanography, Elsevier Pub. Co.
6. Instruction Bulletin - Type 316 Histogram Current Meter, Braincon Corp., Marion, Mass., U.S.A.
7. Neumann, G. 1968. Ocean Currents, Elsevier Pub. Co.
8. Neumann, G. and Pierson, W. J. 1966. Principles of Physical Oceanography, Prentice-Hall, Inc.
9. Sverdrup, H. U., Johnson, M. W. and Fleming, R. H. 1942. The Oceans, Prentice-Hall, Inc.
10. U. S. Treasury Dept. (Coast Guard). 1928. Bulletin No. 19. The Marion Expedition to Davis Strait and Baffin Bay.
11. U. S. Treasury Dept. (Coast Guard). 1950. Bulletin No. 36. International Ice Observation and Ice Patrol Service in the North Atlantic Ocean.

TABLE I

CURRENT METER POSITIONS AND OPERATING TIMES

SUB-STATION	N. LAT.	W. LONG.	WATER DEPTH (M)	INST. DEPTH (M)	INST. SERIAL NO.	TIME SET JUNE 6, 1971 (NDT)	TIME RECOVERED JUNE 9, 1971 (NDT)	TOTAL TIME (HRS : MIN)
A1	50.29.5	52.33.8	226	18	201	11:04	14:53	75:49
A2	"	"	"	28	197	11:25	14:56	75:31
A3	"	"	"	106	123	11:30	14:59	75:29
A4	"	"	"	218	193	11:32	15:03	75:31
B1*	50.29.9	52.32.5	221	13	035	13:22	14.07	72:45
B2	"	"	"	63	124	14:03	14:15	72:12
C1	50.30	52.30	220	15	146	15:52	13:40	69:48
C2	"	"	"	65	139	16:02	13:35	39:33
D1	50.37	52.30.4	201	15	024	17:50	12:34	66:44
D2*	"	"	"	17	182	17:50	12:34	66:44

TABLE II

A1, C1 AND D1 PERIOD AND AMPLITUDE INFORMATION

SUB-STATIONS	AVERAGE PERIOD N-S HRS.	AVERAGE PERIOD E-W HRS.	AVERAGE PERIOD HRS.	AVERAGE OF LAGS HRS.	AV. LAG / AV. PERIOD	AV. N-S AMP. / AV. E-W AMP.
A1	15.1	15.4	15.3	3.3	0.22	1.08
C1	15.9	15.7	15.8	3.4	0.21	1.04
D1	15.5	14.9	15.2	3.3	0.22	1.02

TABLE III

A1, A2, A3 AND A4 PERIOD AND AMPLITUDE INFORMATION

SUB-STATIONS	AVERAGE PERIOD N-S HRS.	AVERAGE PERIOD E-W HRS.	AVERAGE PERIOD HRS.	AVERAGE OF LAGS HRS.	AV. LAG / AV. PERIOD	AV. N-S AMP. / AV. E-W AMP.
A1	15.1	15.4	15.3	3.3	0.22	1.08
A2	15.6	15.1	15.4	3.8	0.25	1.04
A3	13.3	13.4	13.4	2.9	0.21	0.91

TABLE IV

SPATIAL CORRELATIONS

SUB-STATIONS	DEPTHS (M)	SPATIAL CORRELATIONS	
		E-W	N-S
A1-A2	18-28	0.79	0.87
A1-A3	18-106	-0.33	-0.46
A1-A4	18-218	0.19	0.02
A2-A3	28-106	-0.12	-0.42
A2-A4	28-218	0.38	0.00
A3-A4	106-218	0.55	0.57
C1-C2	15-65	0.40	0.45
C1-D1	15-15	0.68	0.64
B2-C2	63-65	0.73	0.79
A1-D1	18-15	0.66	0.65
A1-C1	18-15	0.86	0.86
A2-D1	28-15	0.69	0.58
A2-C1	28-15	0.81	0.79

TABLE V

STATION POSITIONS

STATION	LATITUDE	LONGITUDE
1	50° 00'	50° 00'
2	49° 54'	50° 12'
3	49° 47'	50° 30'
4	49° 42'	50° 39'
5	49° 35'	51° 00'
6	49° 22'	51° 30'
7	49° 09'	52° 00'
8	48° 55'	52° 34'

TABLE VI

YEAR	DEPTH	LATITA	LATITB	DISTANCE	REL VEL	ABS VEL
1970	0	50,039	49,917	25000,89	0,0	-0,100
1970	10	50,039	49,917	25000,89	-0,004	-0,104
1970	50	50,039	49,917	25000,89	-0,018	-0,118
1970	100	50,039	49,917	25000,89	0,011	-0,089
1970	200	50,039	49,917	25000,89	0,079	-0,021
1970	300	50,039	49,917	25000,89	0,100	0,000
1970	0	49,917	49,783	27091,47	0,0	0,063
1970	10	49,917	49,783	27091,47	-0,003	0,060
1970	50	49,917	49,783	27091,47	0,017	0,080
1970	100	49,917	49,783	27091,47	-0,003	0,060
1970	200	49,917	49,783	27091,47	-0,063	0,000
1970	300	49,917	49,783	27091,47	-0,070	-0,007
1970	0	49,783	49,700	14150,52	0,0	0,038
1970	10	49,783	49,700	14150,52	0,0	0,038
1970	50	49,783	49,700	14150,52	-0,133	-0,095
1970	100	49,783	49,700	14150,52	-0,083	-0,045
1970	200	49,783	49,700	14150,52	-0,019	0,019
1970	300	49,783	49,700	14150,52	-0,038	-0,000
1970	0	49,700	49,583	28264,69	0,0	0,016
1970	10	49,700	49,583	28264,69	-0,003	0,013
1970	50	49,700	49,583	28264,69	0,010	0,026
1970	100	49,700	49,583	28264,69	-0,003	0,013
1970	200	49,700	49,583	28264,69	-0,016	0,000
1970	300	49,700	49,583	28264,69	-0,006	0,010
1970	0	49,583	49,367	43246,40	0,0	0,192
1970	10	49,583	49,367	43246,40	-0,017	0,175
1970	50	49,583	49,367	43246,40	-0,038	0,154
1970	100	49,583	49,367	43246,40	-0,077	0,115
1970	200	49,583	49,367	43246,40	-0,154	0,038
1970	300	49,583	49,367	43246,40	-0,192	-0,000
1970	0	49,367	49,150	43439,80	0,0	0,156
1970	10	49,367	49,150	43439,80	-0,002	0,154
1970	50	49,367	49,150	43439,80	-0,031	0,125
1970	100	49,367	49,150	43439,80	-0,052	0,104
1970	200	49,367	49,150	43439,80	-0,100	0,056
1970	300	49,367	49,150	43439,80	-0,156	-0,000
1970	0	49,150	48,917	49614,32	0,0	0,026
1970	10	49,150	48,917	49614,32	-0,005	0,021
1970	50	49,150	48,917	49614,32	-0,009	0,017
1970	100	49,150	48,917	49614,32	-0,018	0,008
1970	200	49,150	48,917	49614,32	-0,026	0,000
1970	300	49,150	48,917	49614,32	-0,007	0,019
1970	0	48,917	48,767	29499,89	0,0	0,025
1970	10	48,917	48,767	29499,89	-0,006	0,019
1970	50	48,917	48,767	29499,89	0,006	0,031
1970	100	48,917	48,767	29499,89	-0,025	0,000
1969	0	50,000	49,900	19975,95	0,0	-0,004
1969	10	50,000	49,900	19975,95	0,0	-0,004
1969	50	50,000	49,900	19975,95	0,004	0,000
1969	100	50,000	49,900	19975,95	0,004	0,000
1969	200	50,000	49,900	19975,95	0,004	0,000
1969	300	50,000	49,900	19975,95	0,004	0,000
1969	400	50,000	49,900	19975,95	-0,009	-0,013
1969	500	50,000	49,900	19975,95	-0,013	-0,017
1969	0	49,900	49,783	23077,75	0,0	0,331
1969	10	49,900	49,783	23077,75	0,0	0,331
1969	50	49,900	49,783	23077,75	-0,066	0,265
1969	100	49,900	49,783	23077,75	-0,152	0,179

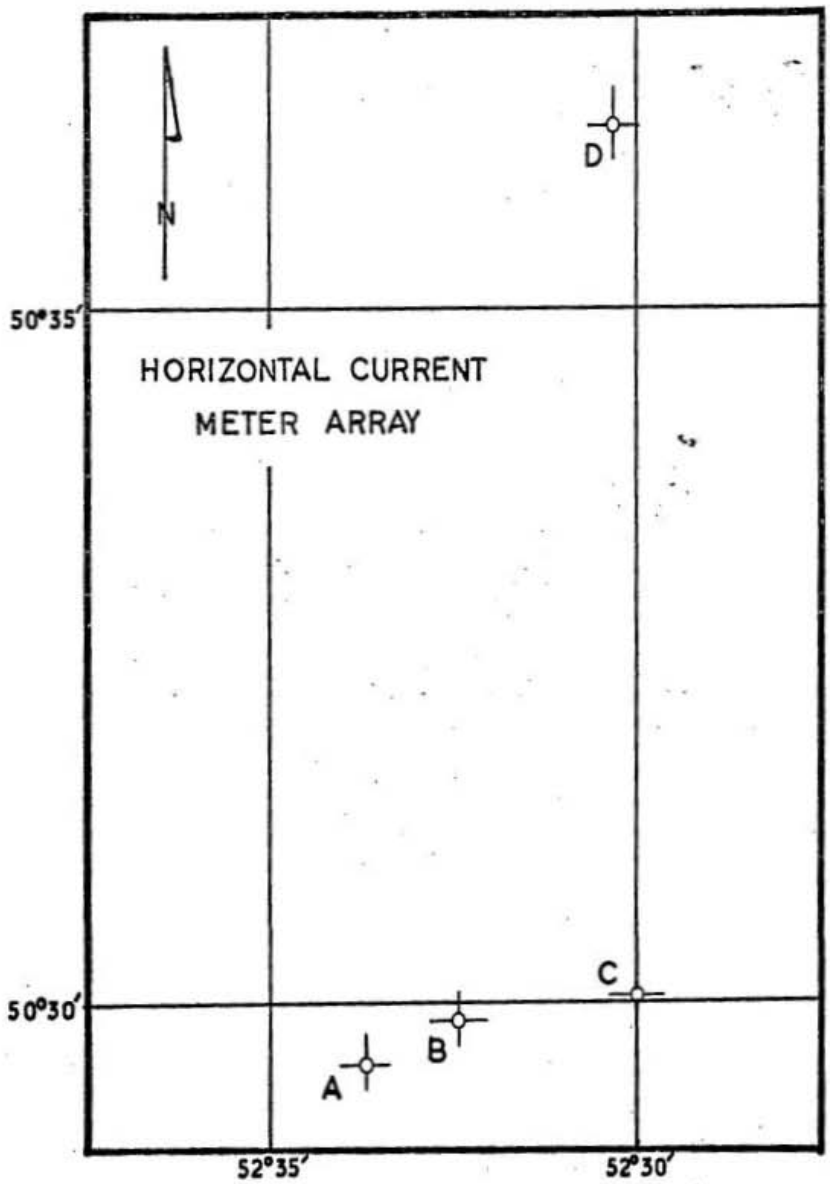

Fig. 1. The horizontal current meter array.

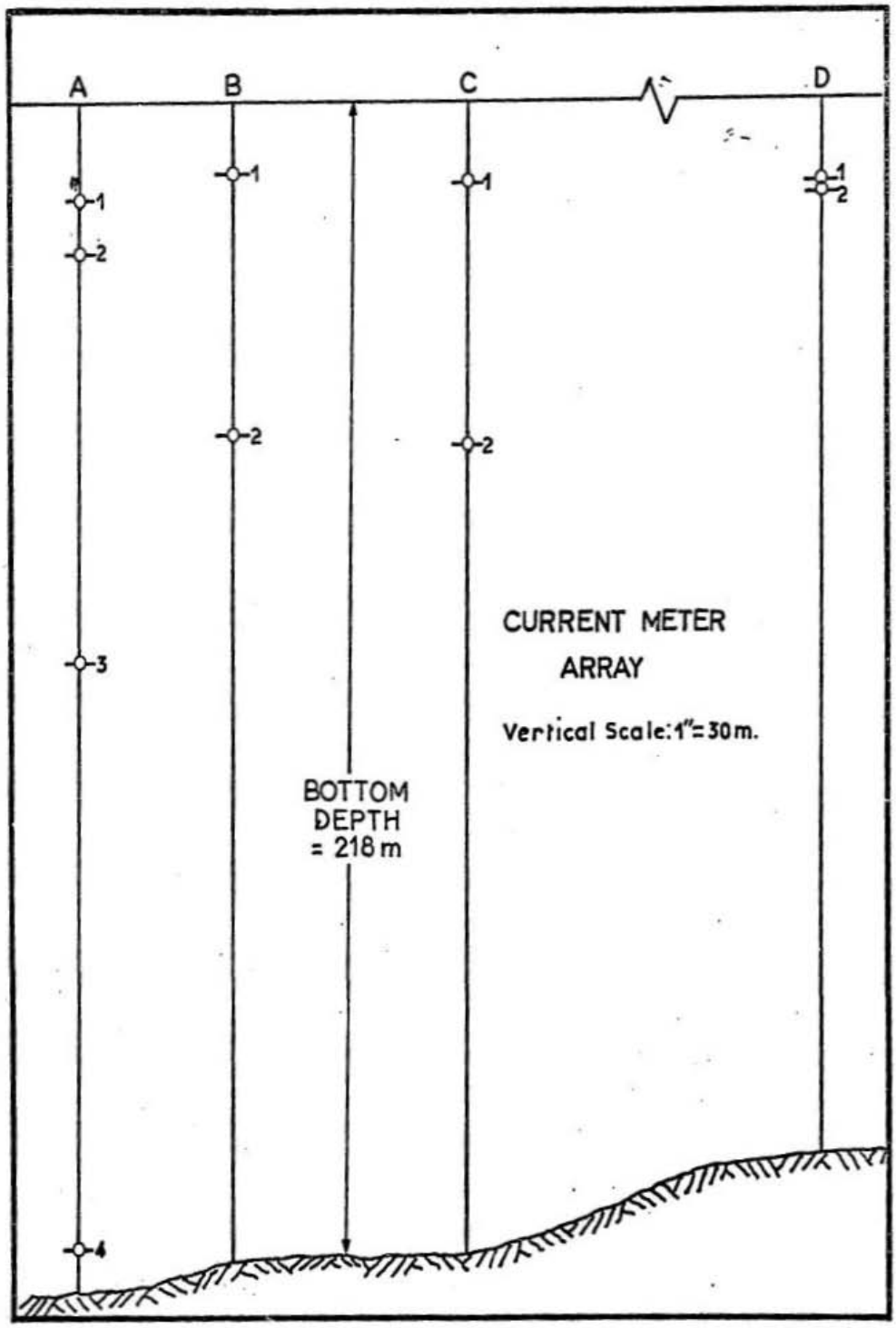

Fig. 2. The vertical current meter array.

3,6

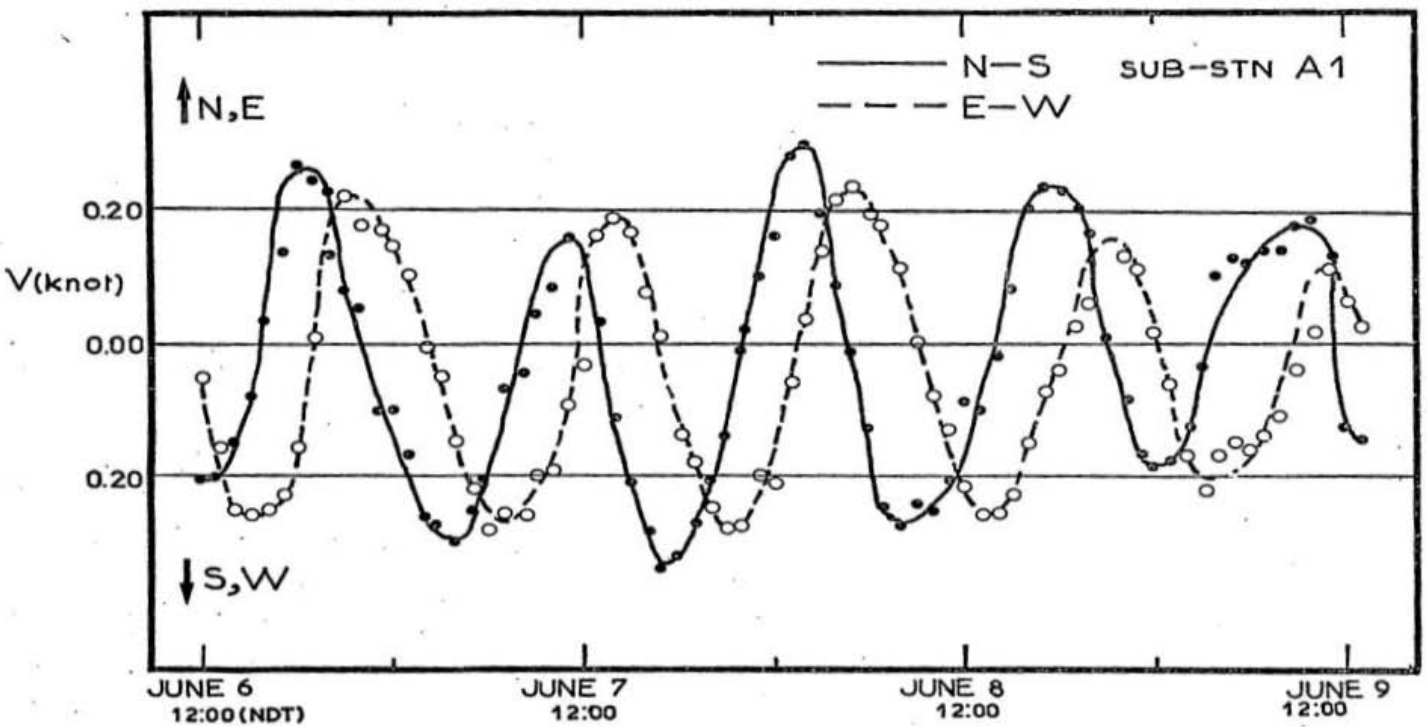

Fig. 3. N-S and E-W current components at sub-station A1 versus time.

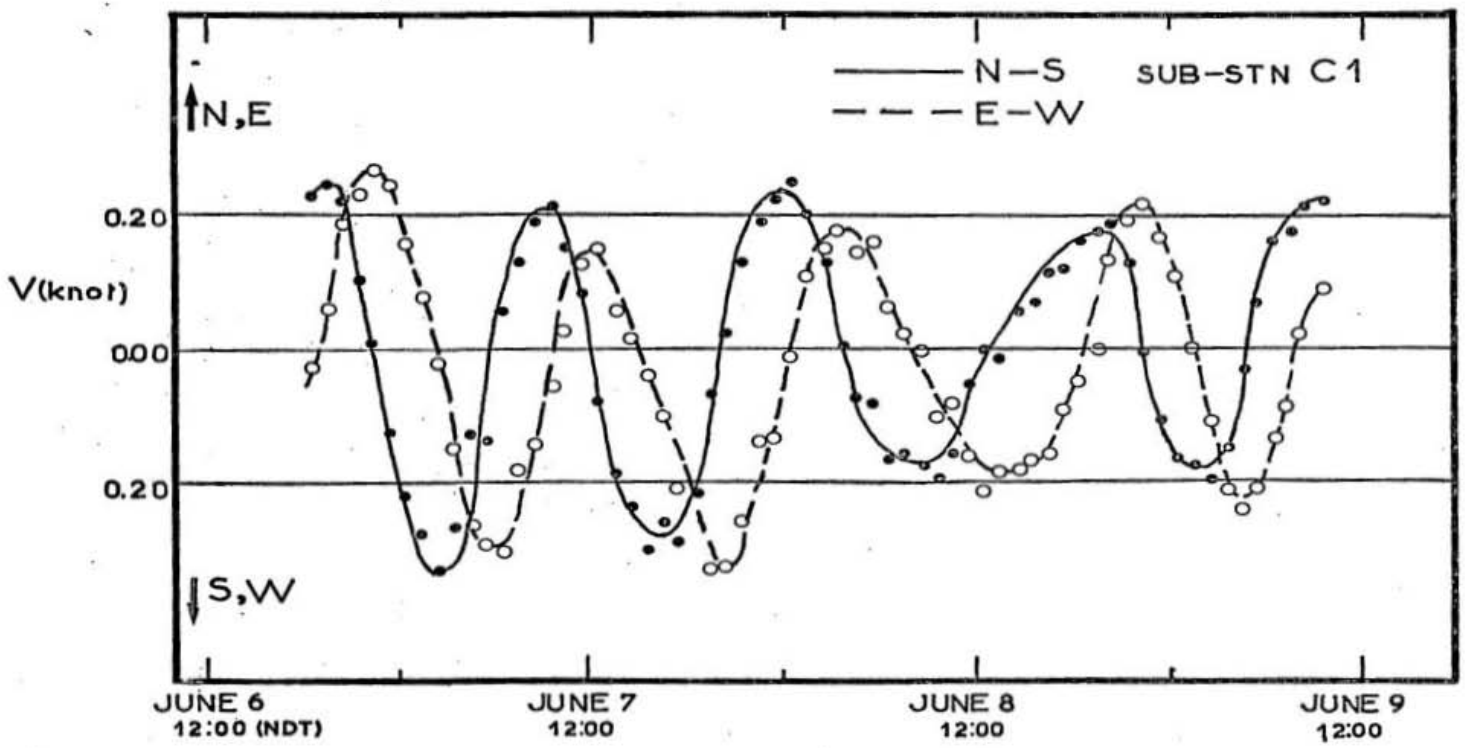

Fig. 4. N-S and E-W current components at sub-station C1 versus time.

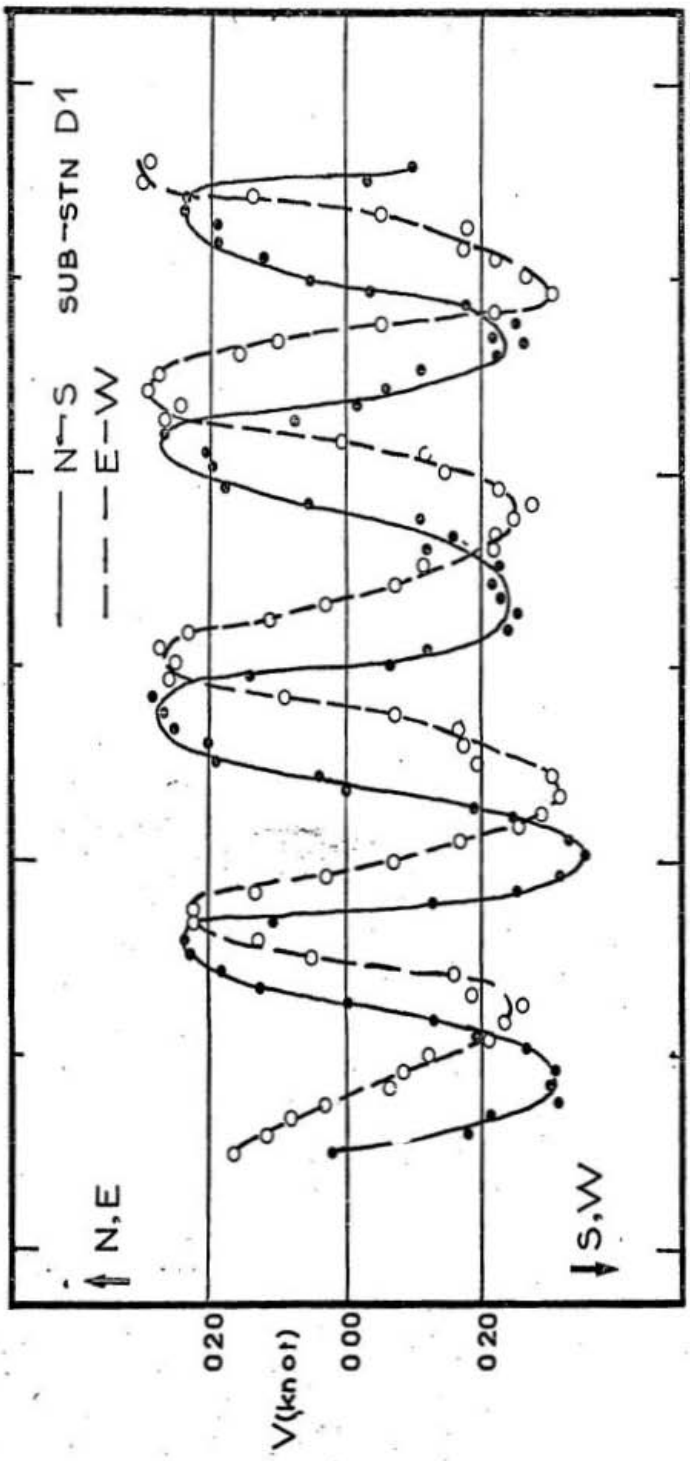

Fig. 5. N-S and E-W current components at sub-station D1 versus time.

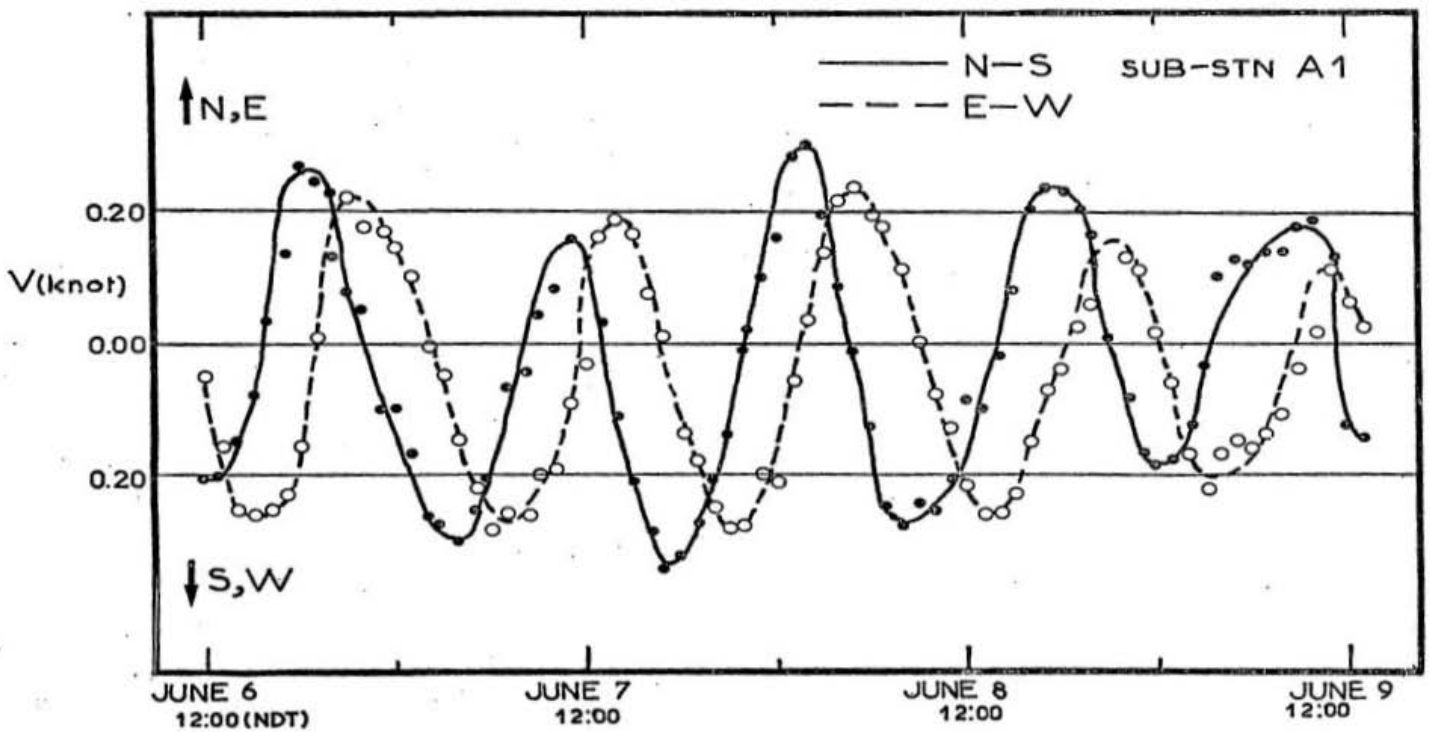

Fig. 6. N-S and E-W current components at sub-station A1 versus time.

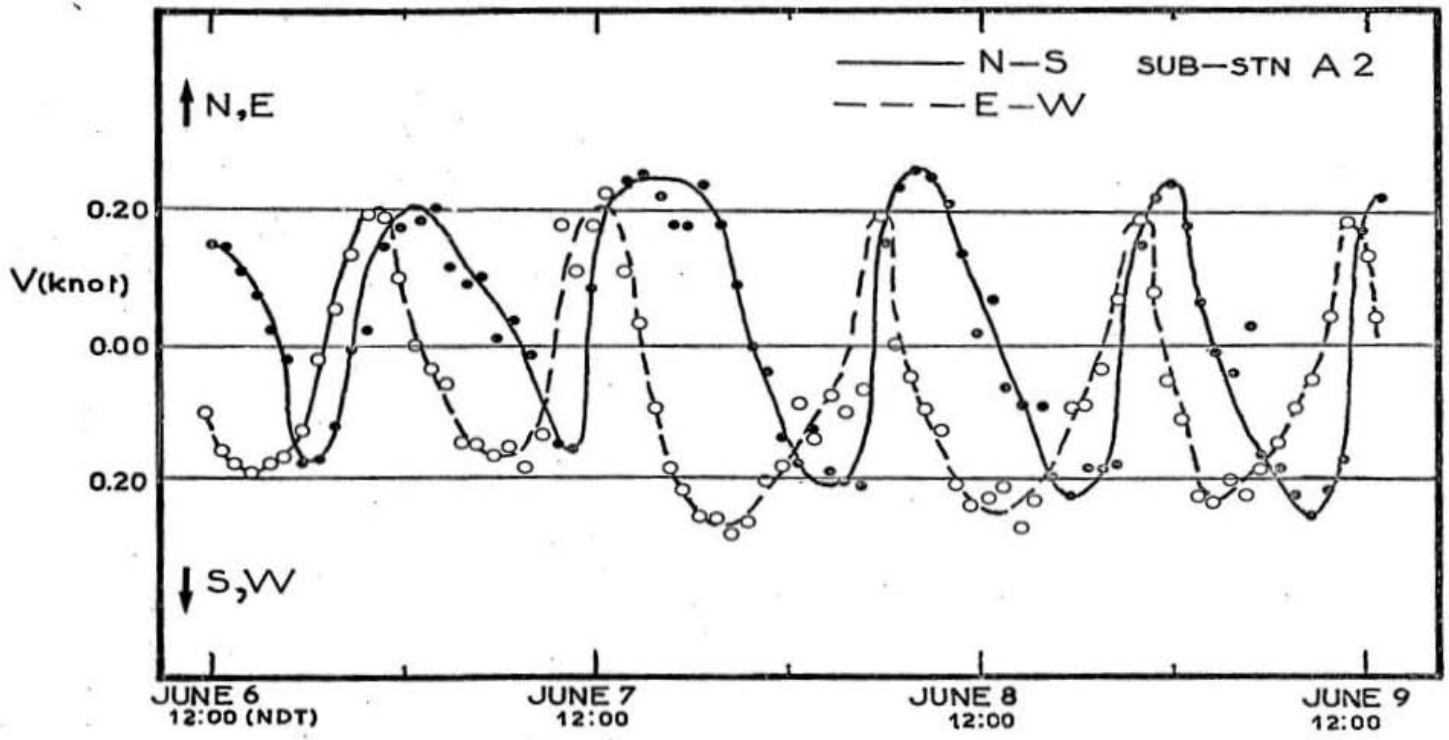

Fig. 7. N-S and E-W current components at sub-station A2 versus time.

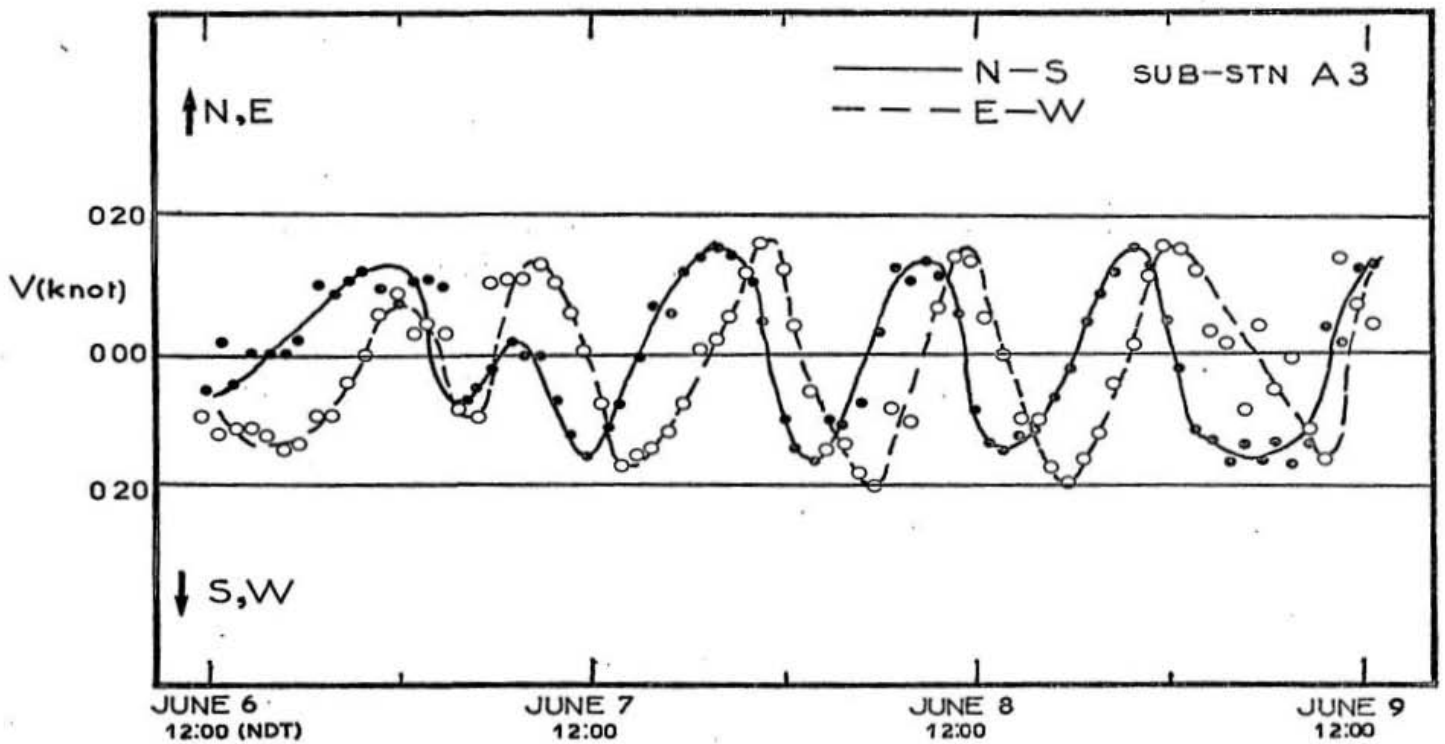

Fig. 8. N-S and E-W current components at sub-station A3 versus time.

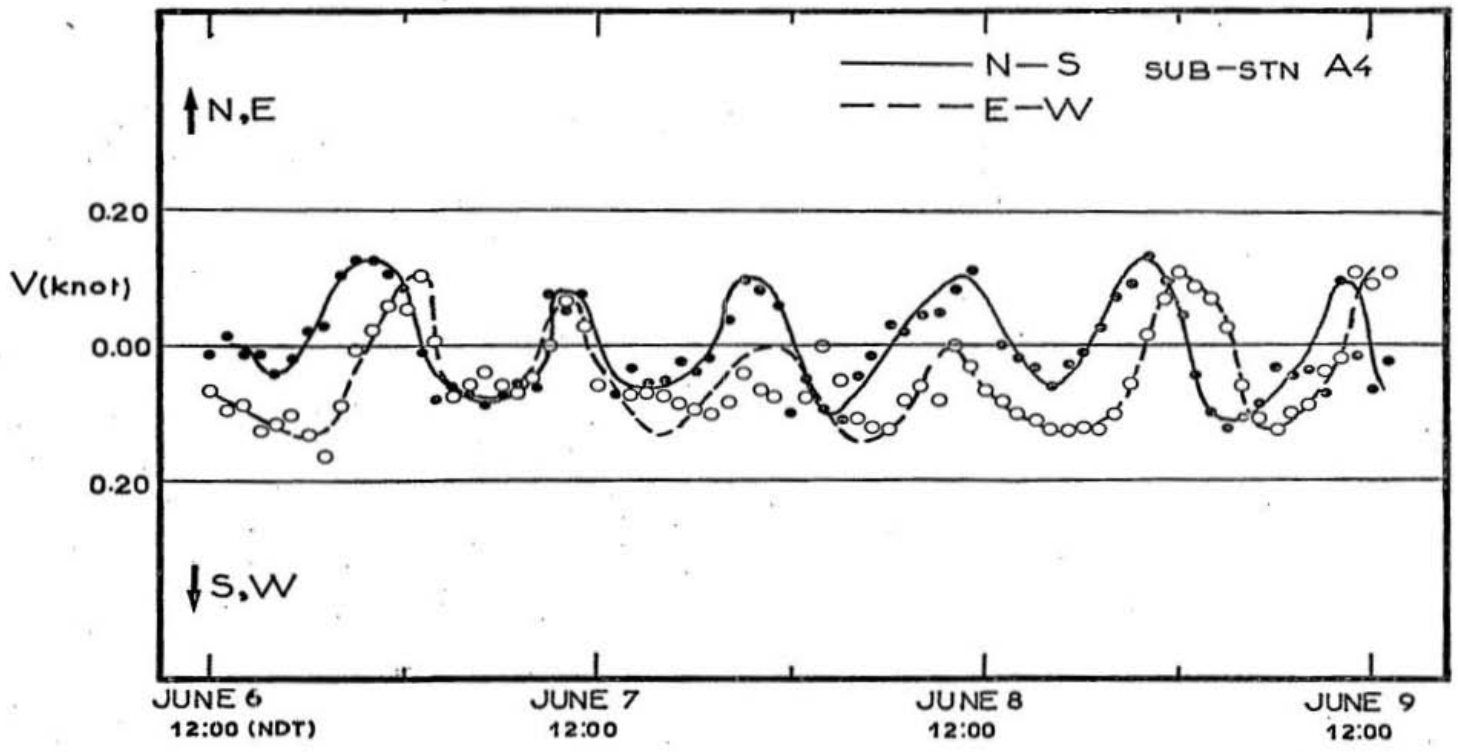

Fig. 9. N-S and E-W current components at sub-station A4 versus time.

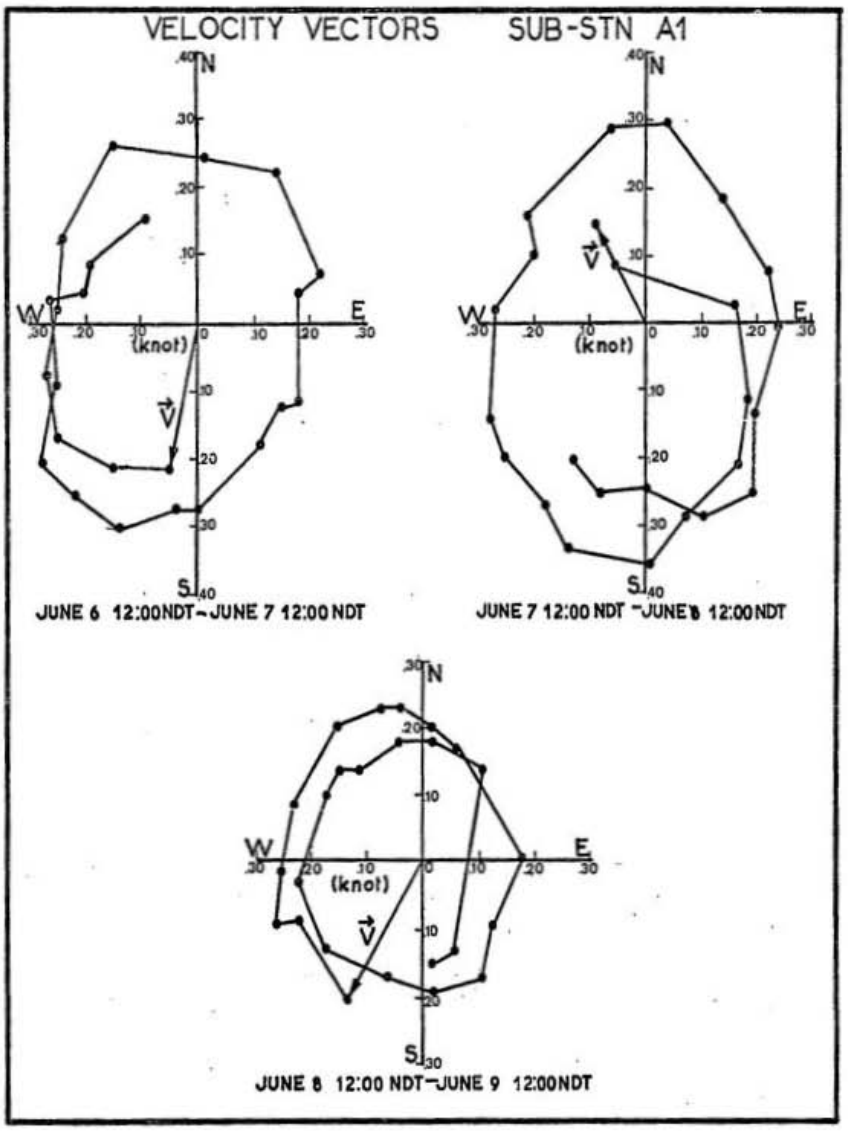

Fig. 10. Velocity vectors at sub-station A1 plotted in current-rose form.

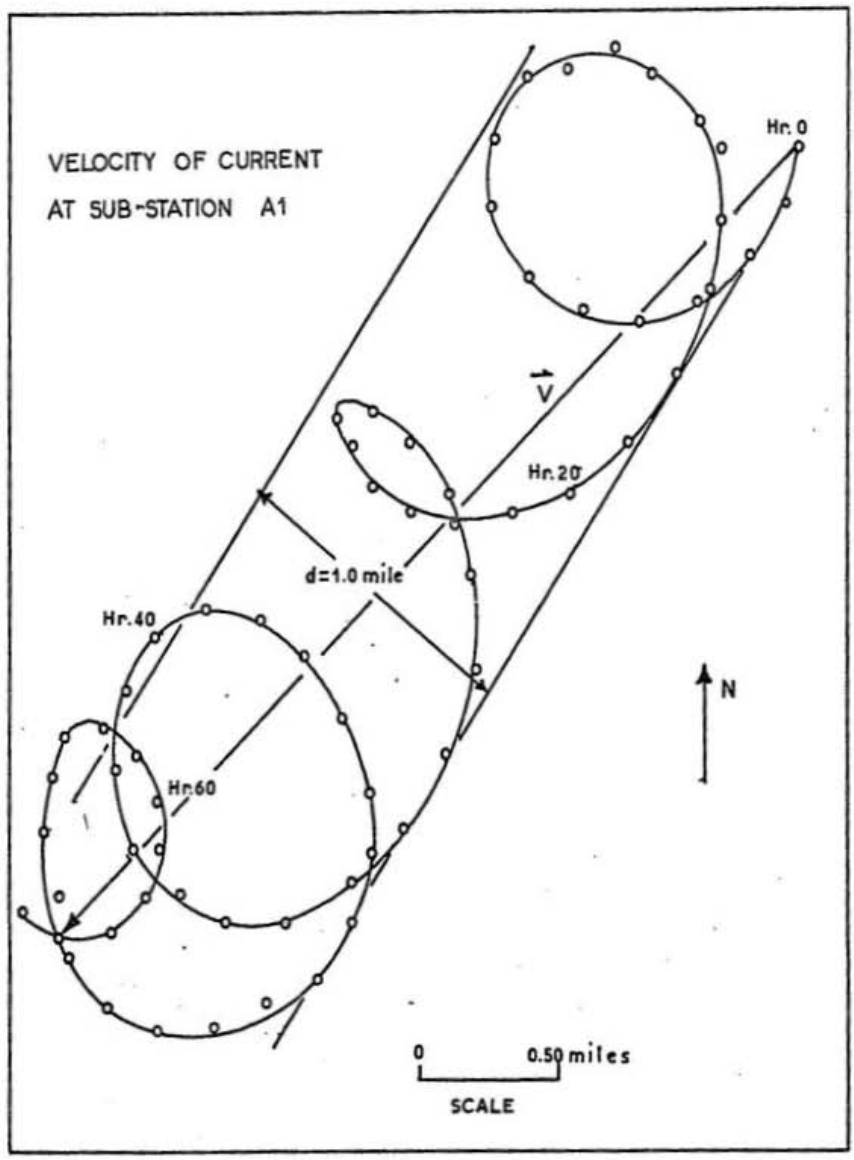

Fig. 11. Cumulative vector diagram for current at sub-station A1.

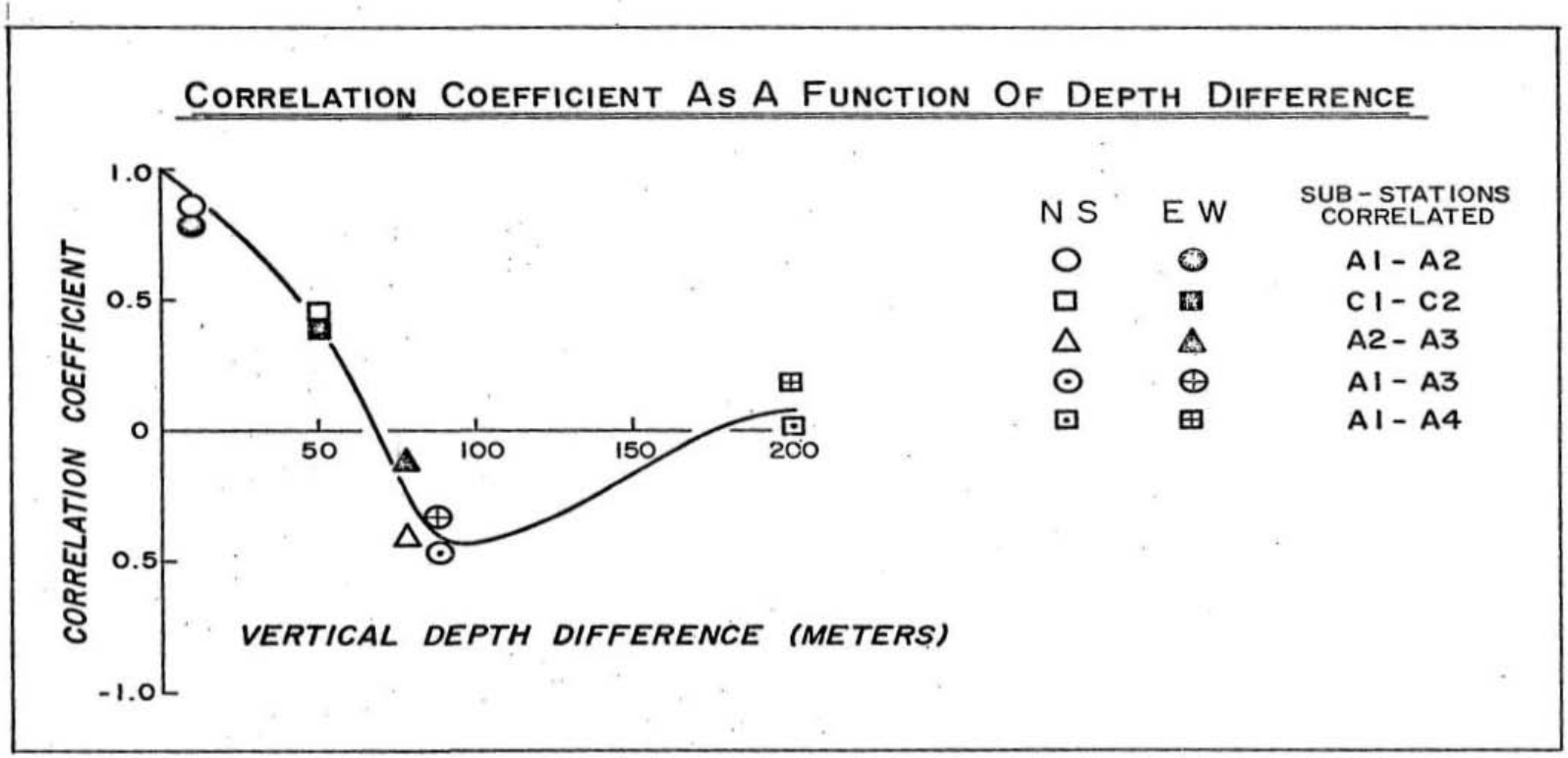

Fig. 12. The correlation coefficient curve as a function of depth difference.

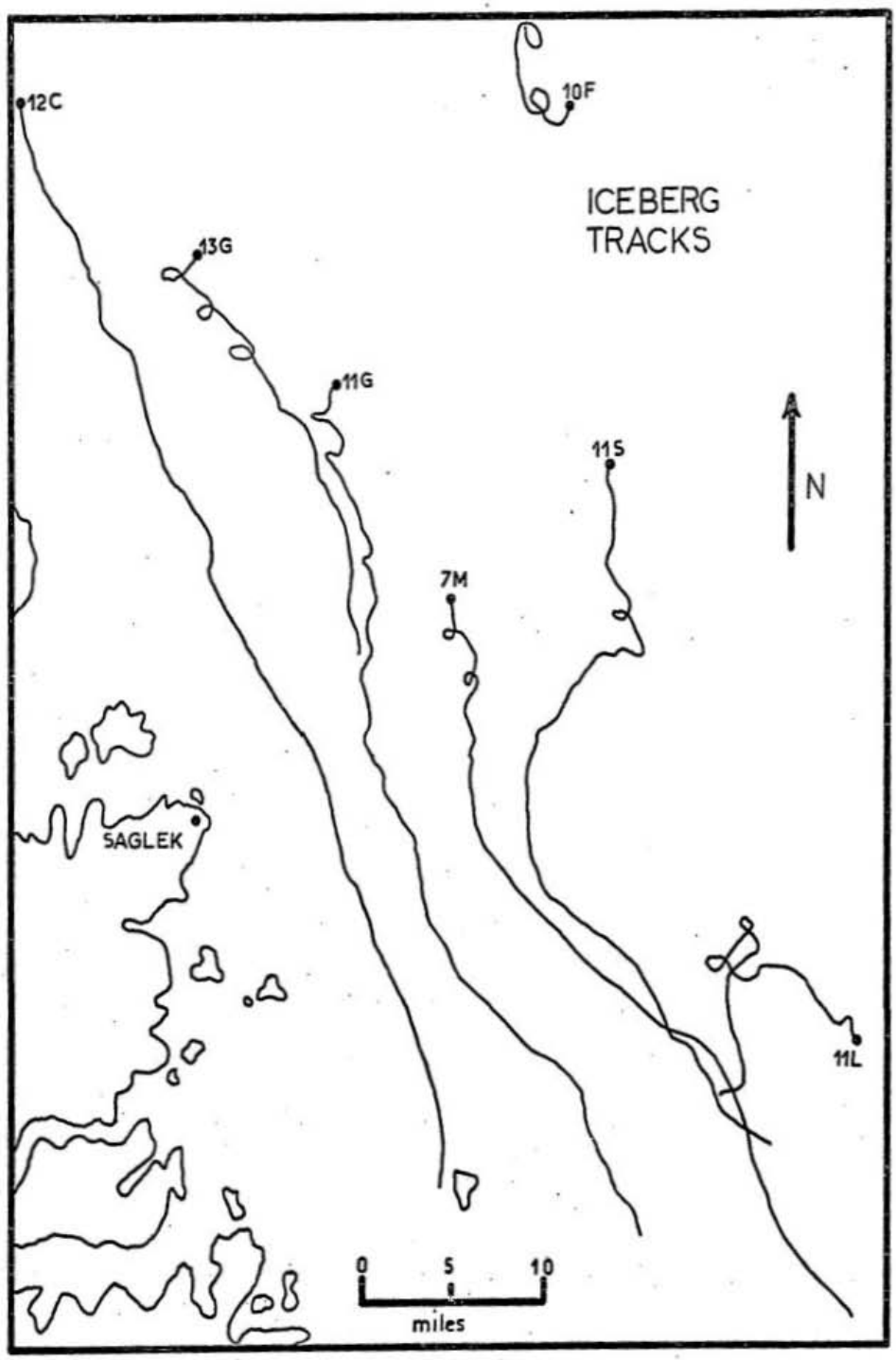

Fig. 13. Drift patterns of icebergs in the Labrador Sea.

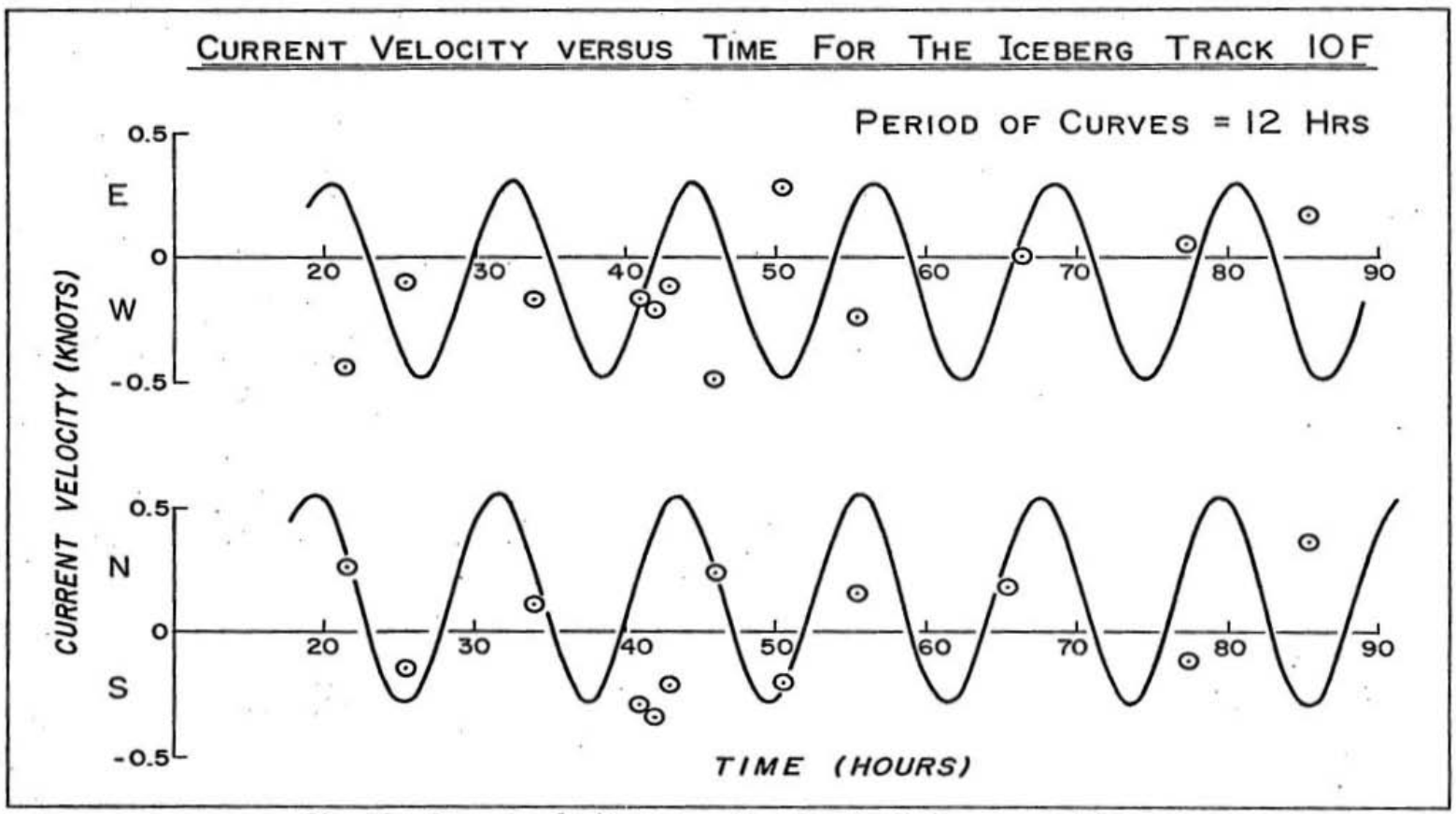

Fig. 14. Current velocity versus time for the iceberg track 10F with imposed sinusoid of period 12 hrs.

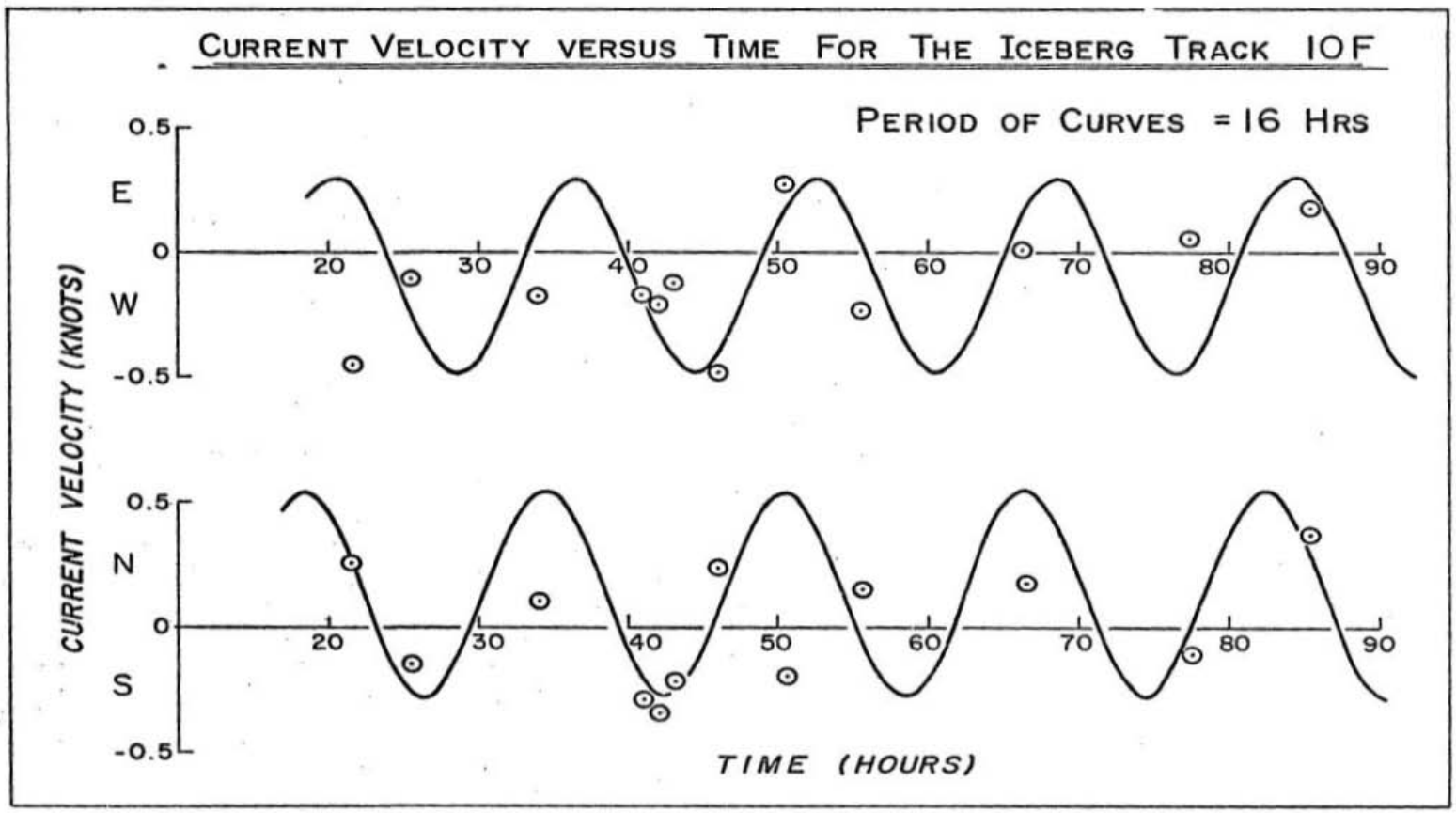

Fig. 15. Current velocity versus time for the iceberg track 10F with imposed sinusoid of period 16 hrs.

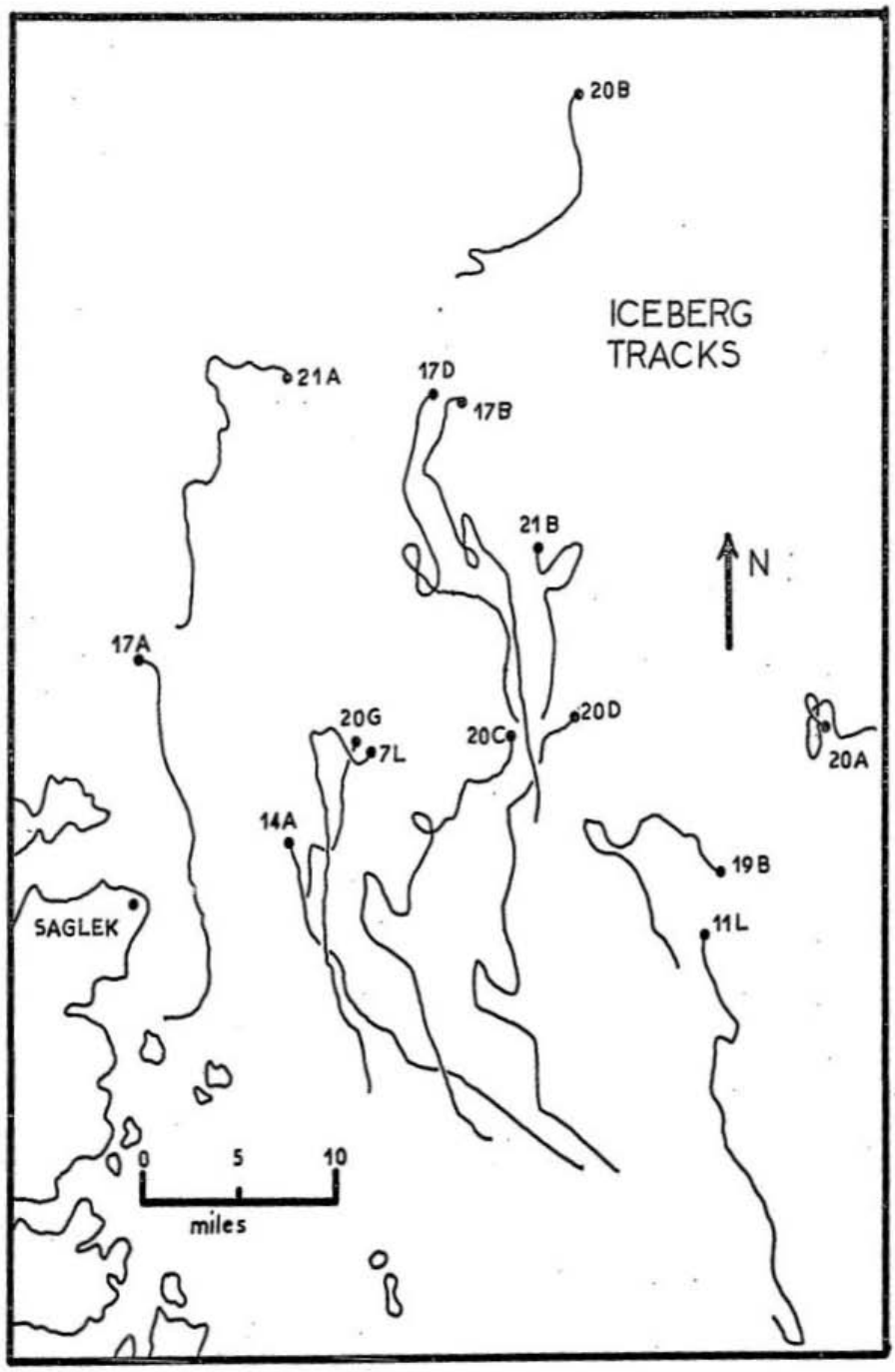

Fig. 16. Drift pattern of icebergs in the Labrador Sea after a pressure disturbance.

17

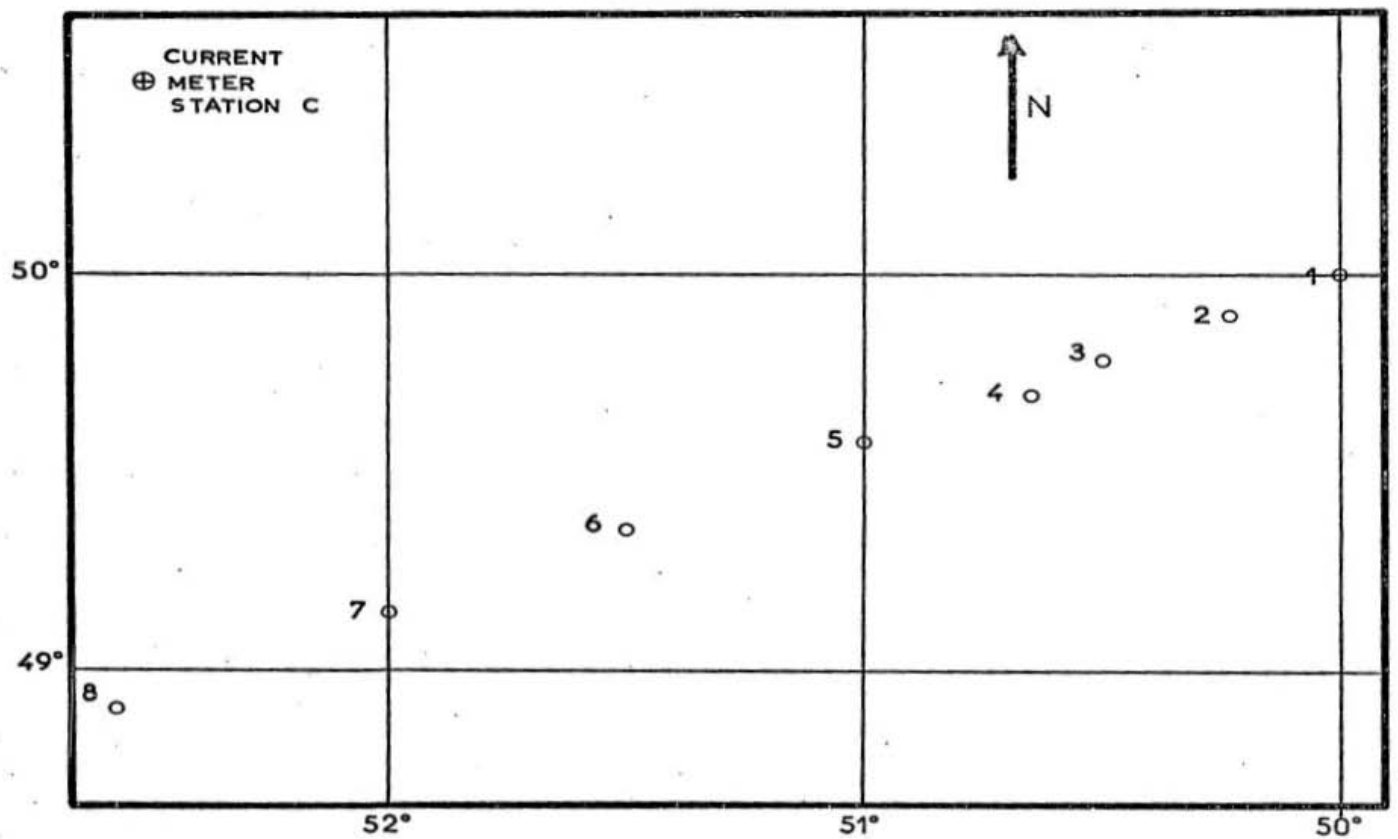

Fig. 17. Station positions for the STD measurements.

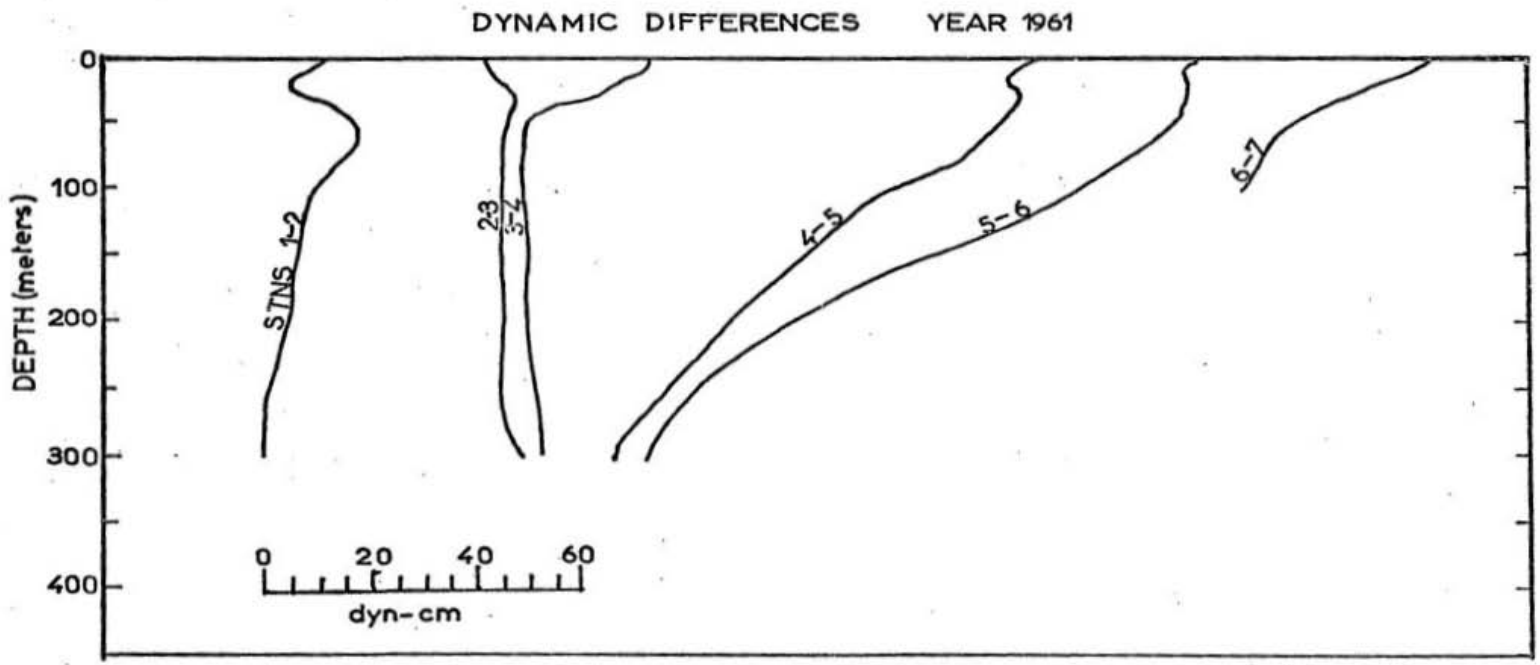

Fig. 18. Dynamic differences versus depth. (1961).

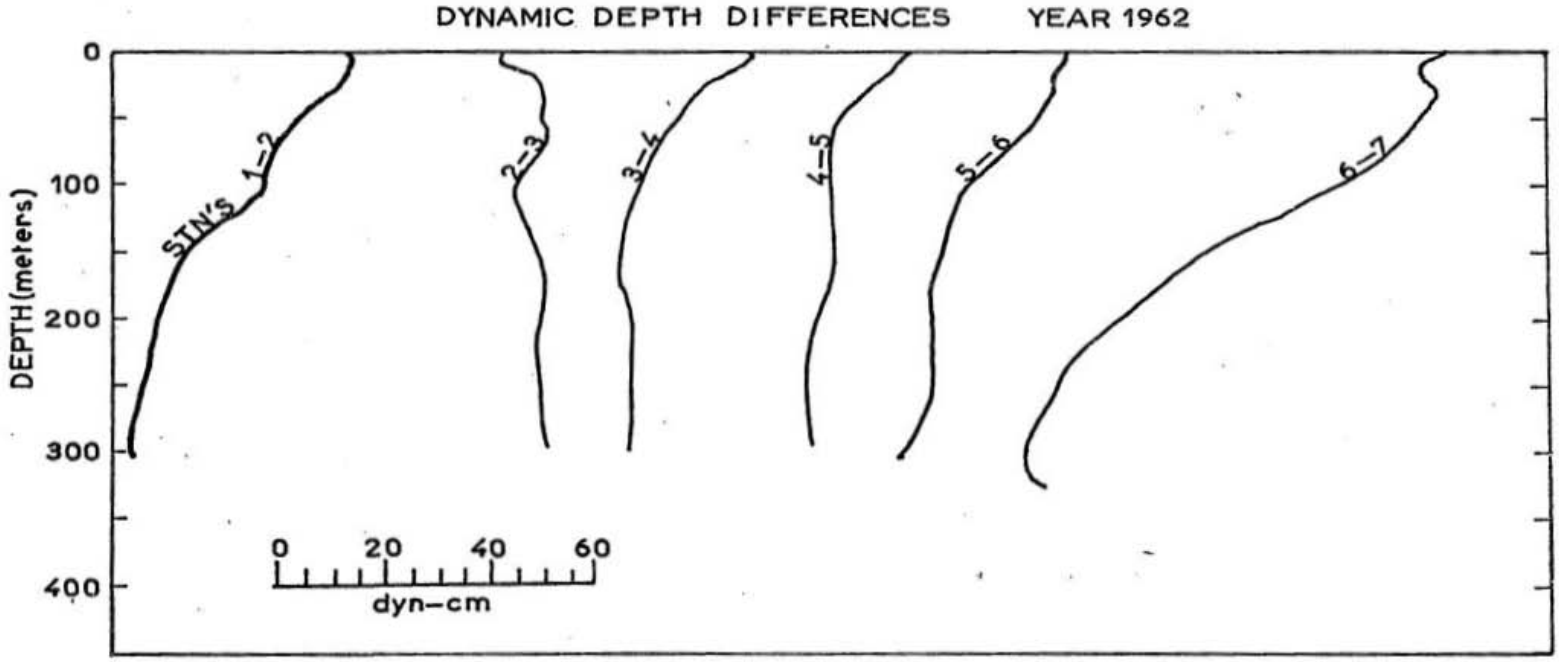

Fig. 19. Dynamic differences versus depth. (1962).

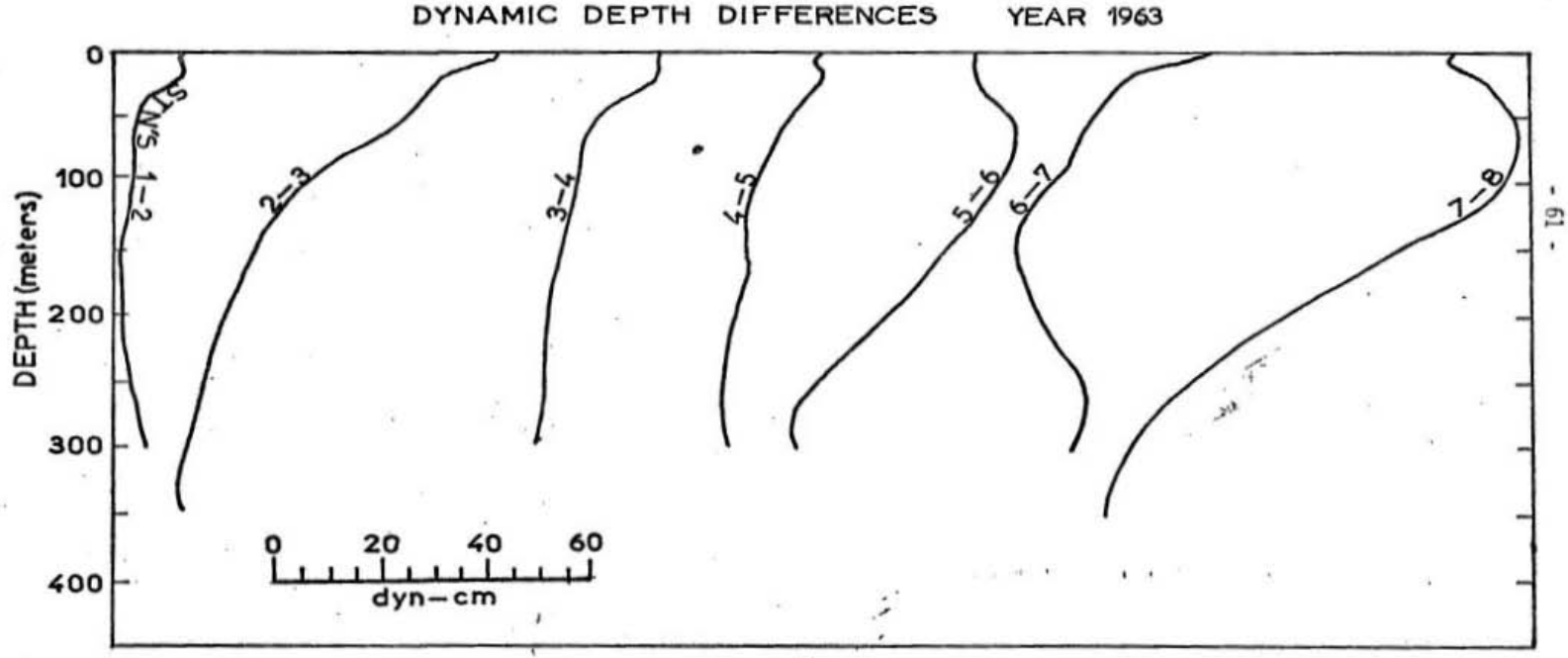

Fig. 20. Dynamic differences versus depth. (1963).

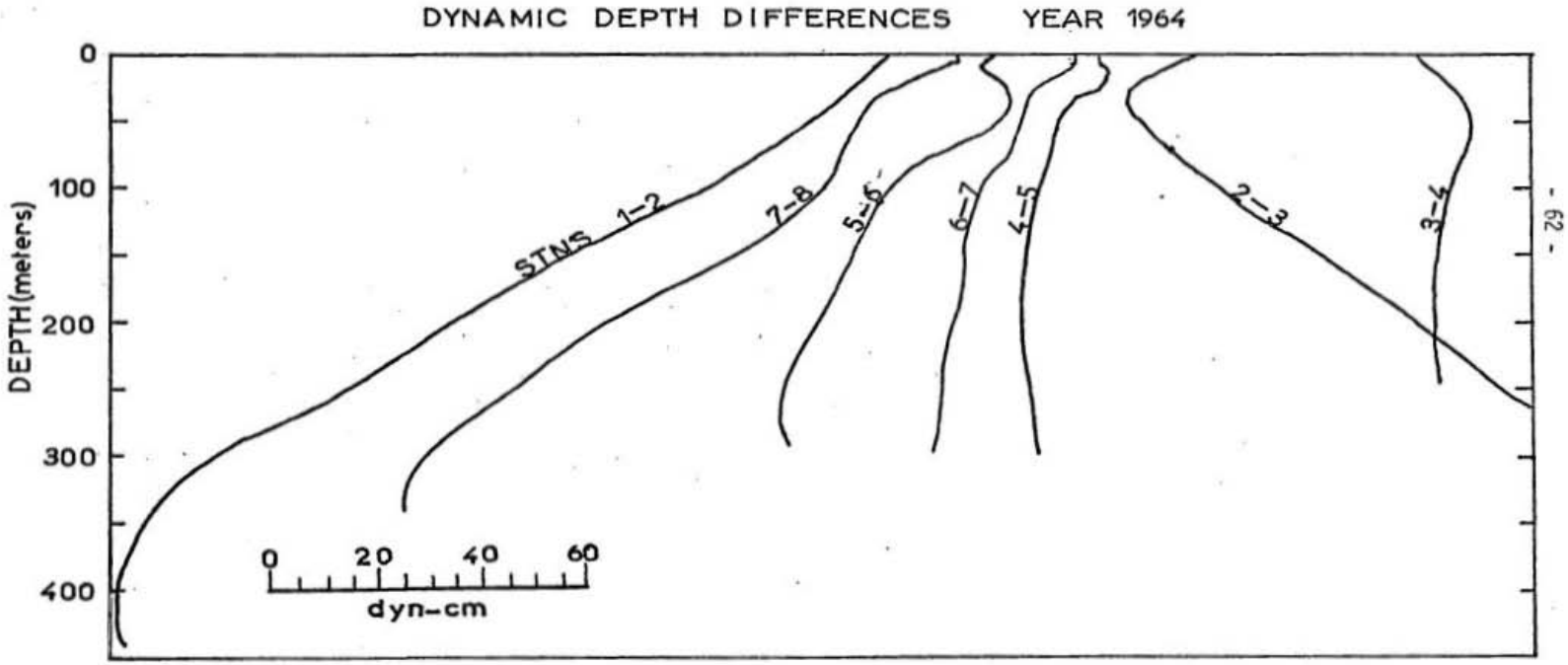

Fig. 21. Dynamic differences versus depth. (1964).

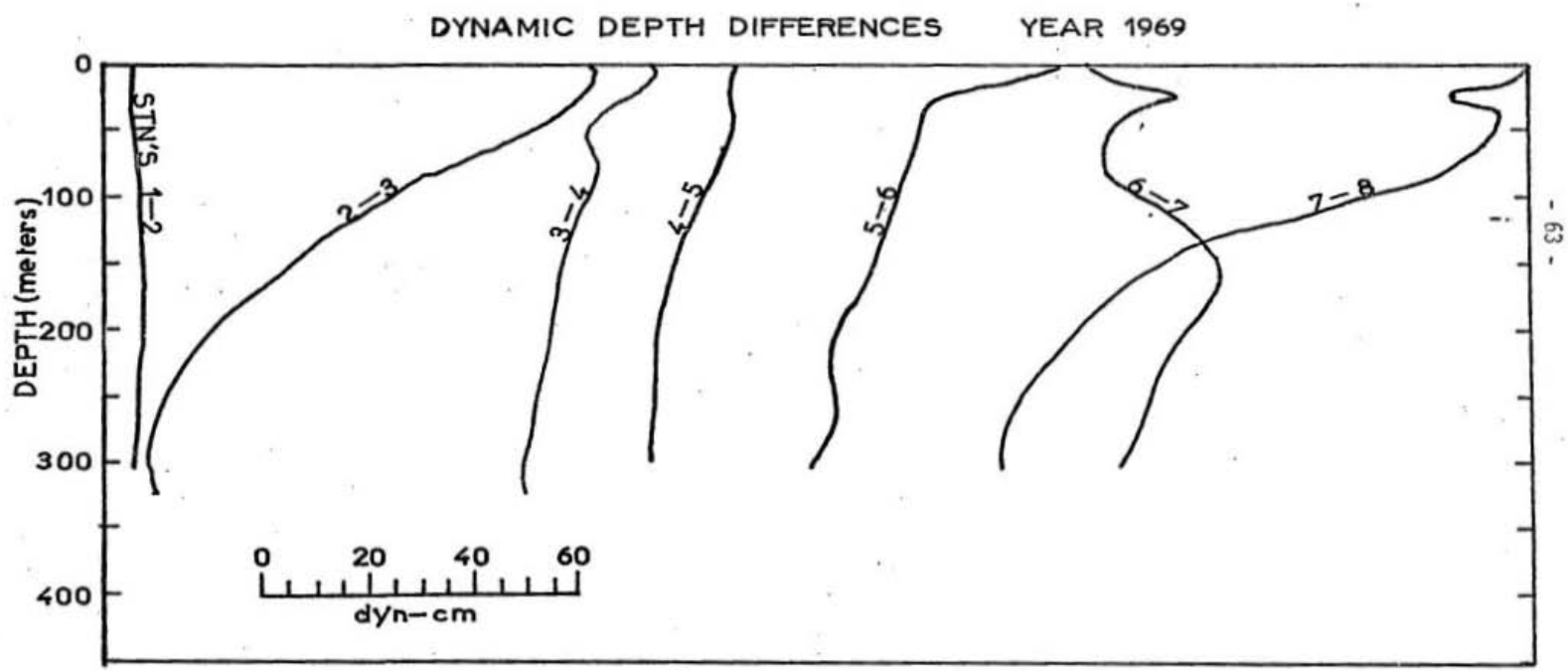

Fig. 22. Dynamic differences versus depth. (1969).

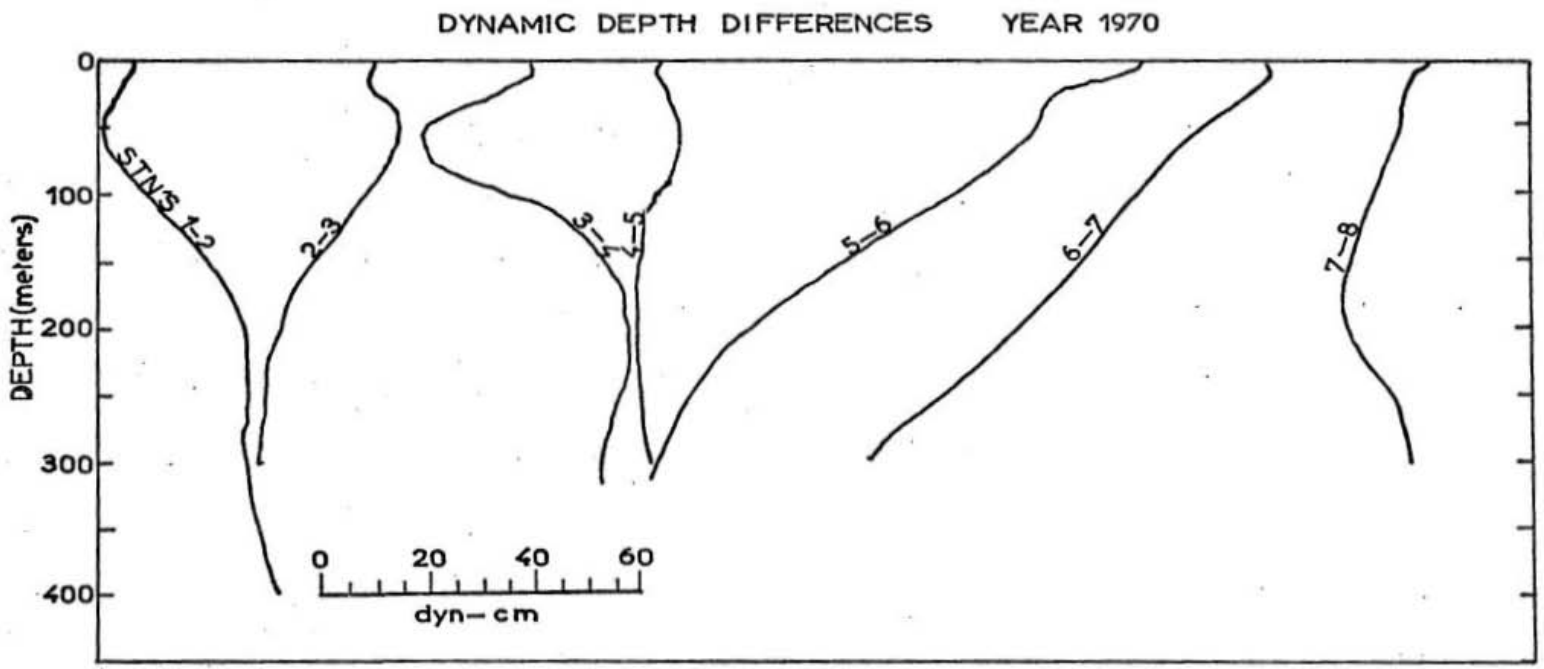

Fig. 23. Dynamic differences versus depth. (1970).

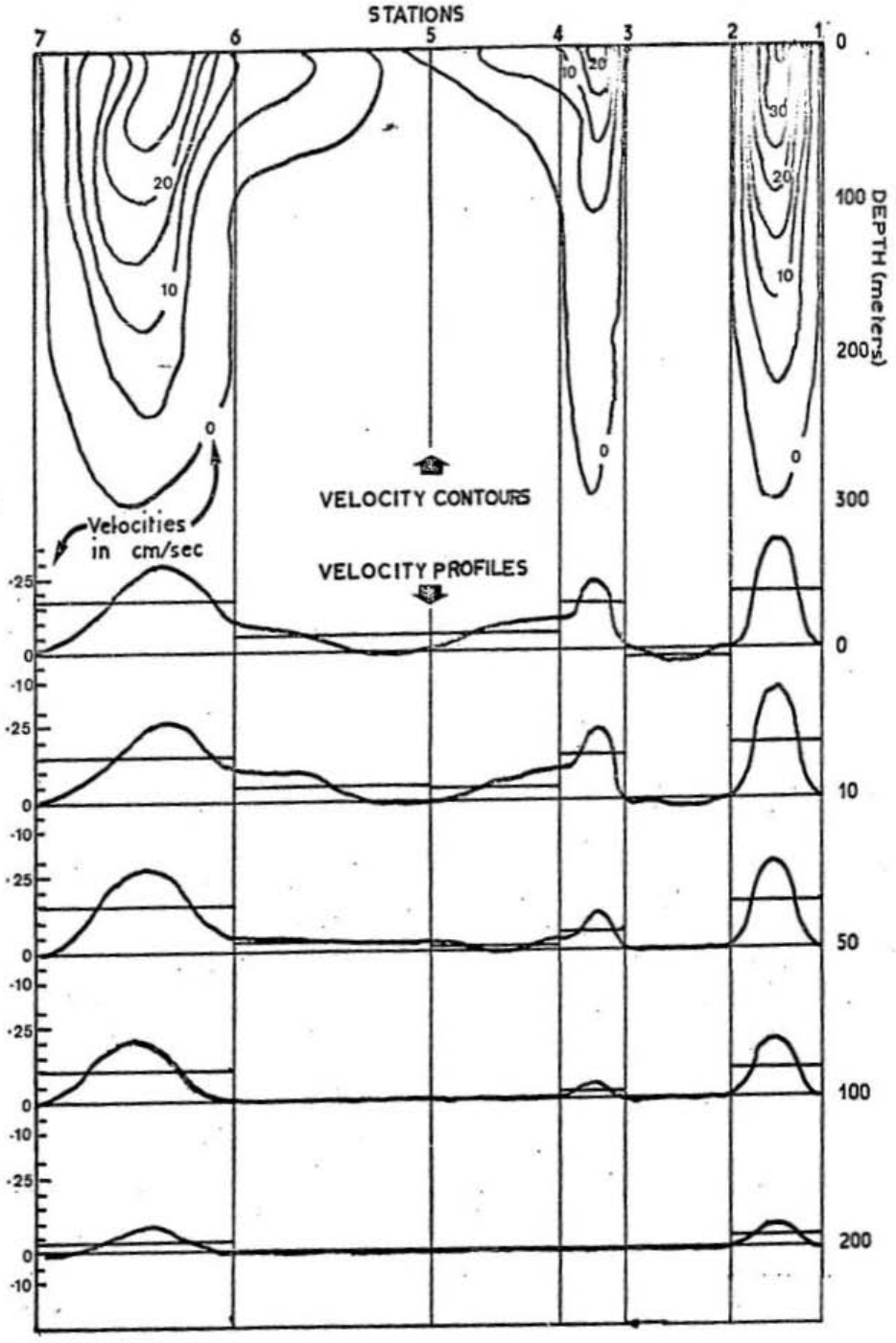

Fig. 24. An example of the method of constructing the velocity contours (using values from the 1962 data).

25

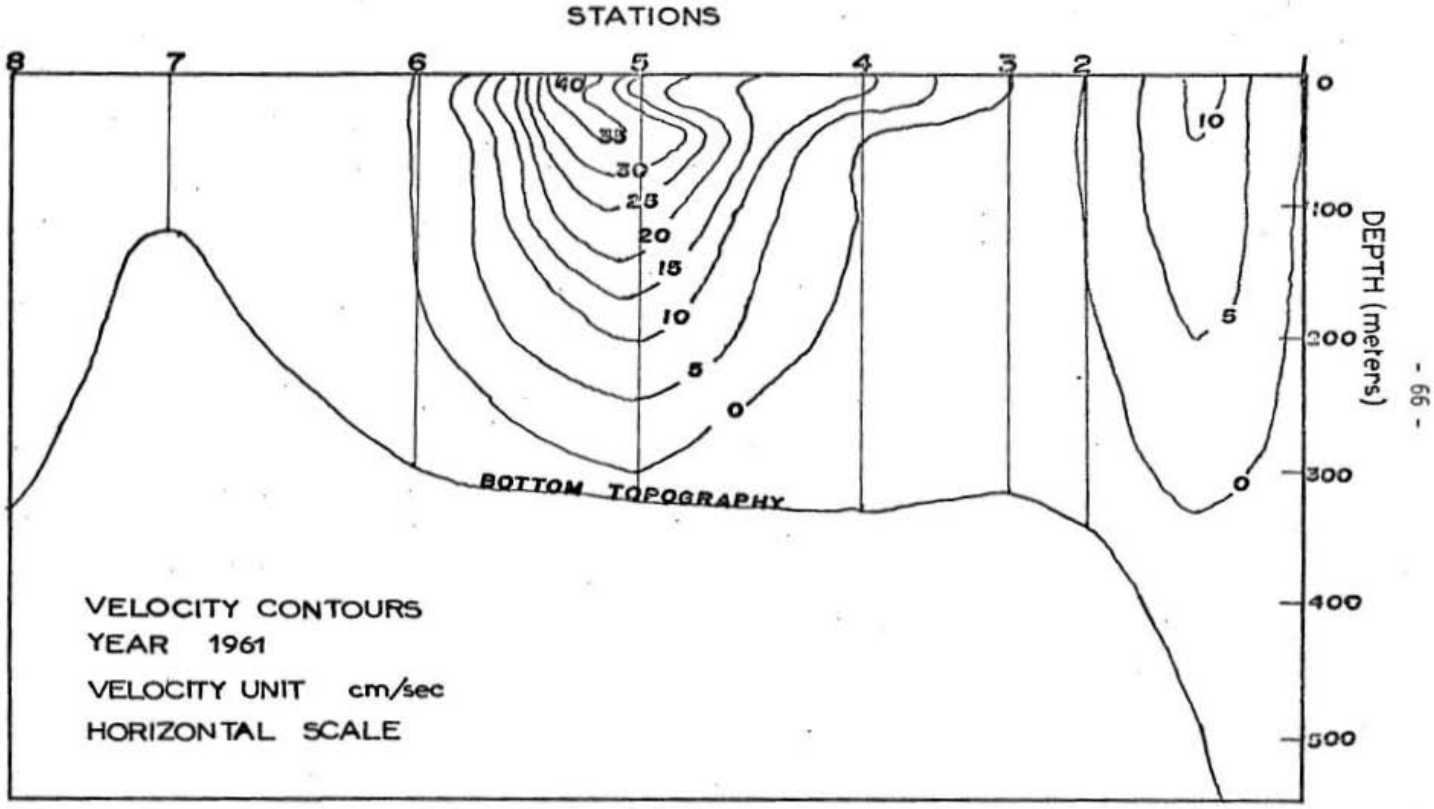

Fig. 25. Velocity contours. (1961).

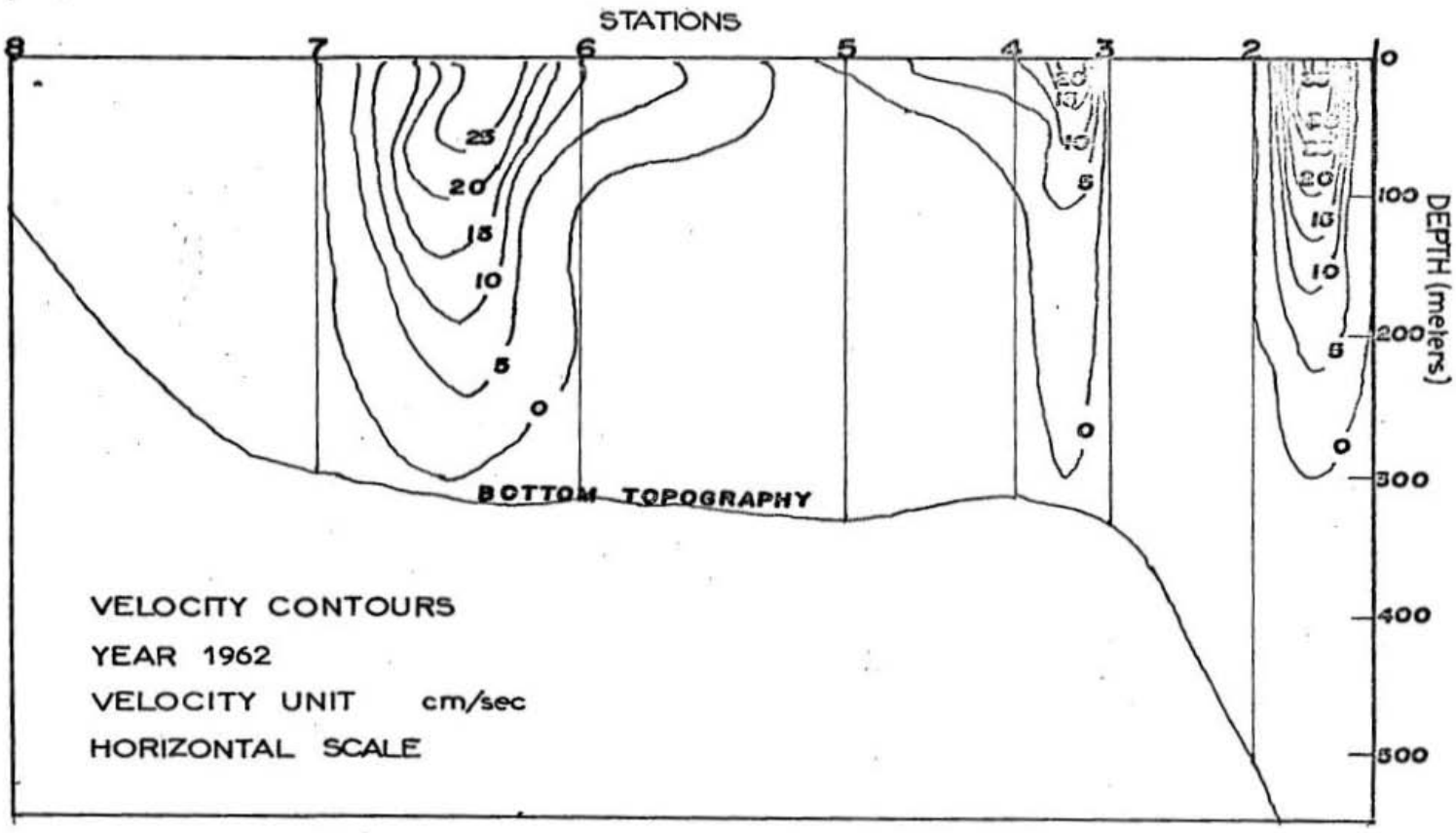

Fig. 26. Velocity contours. (1962).

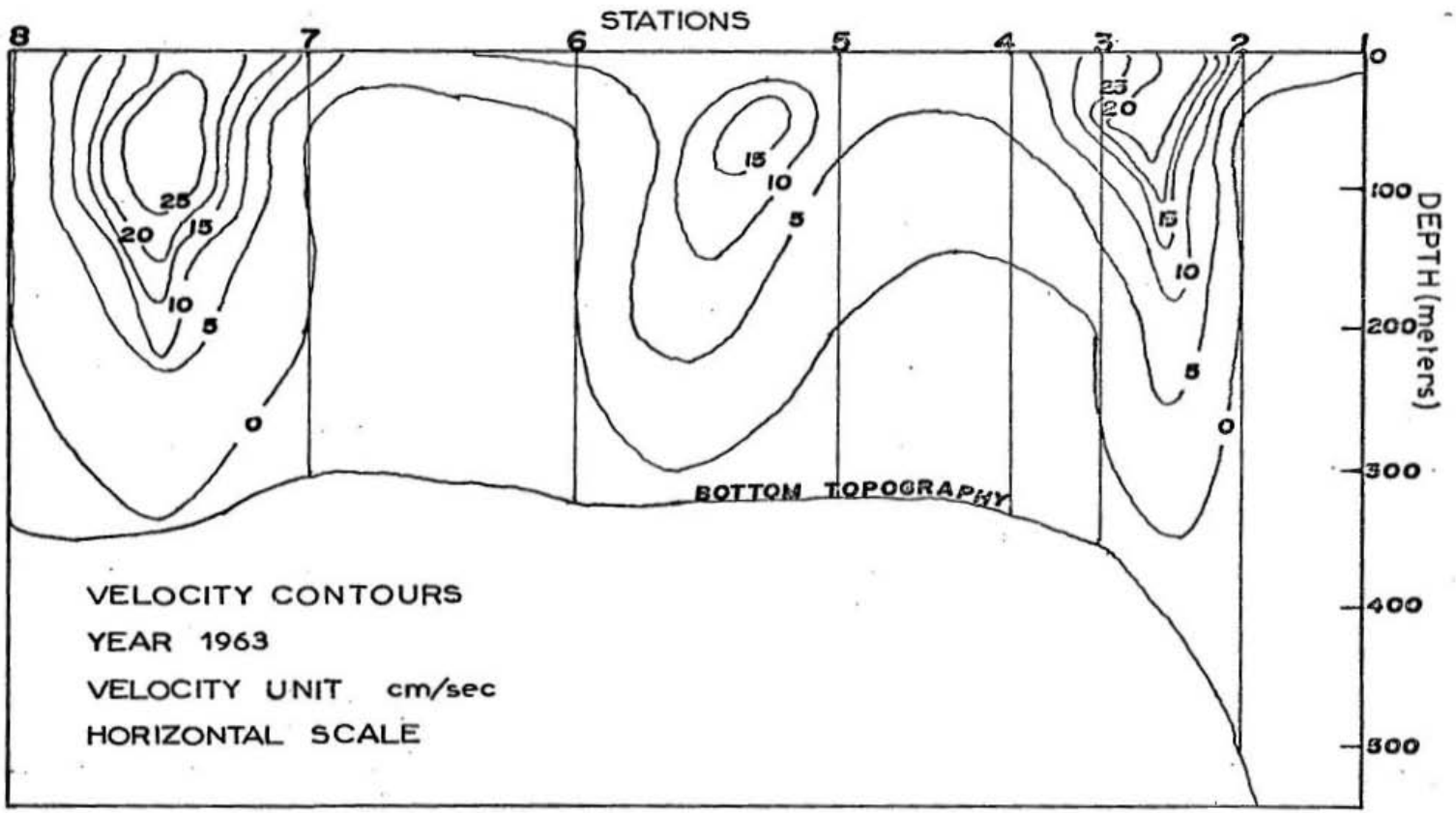

Fig. 27. Velocity contours. (1963).

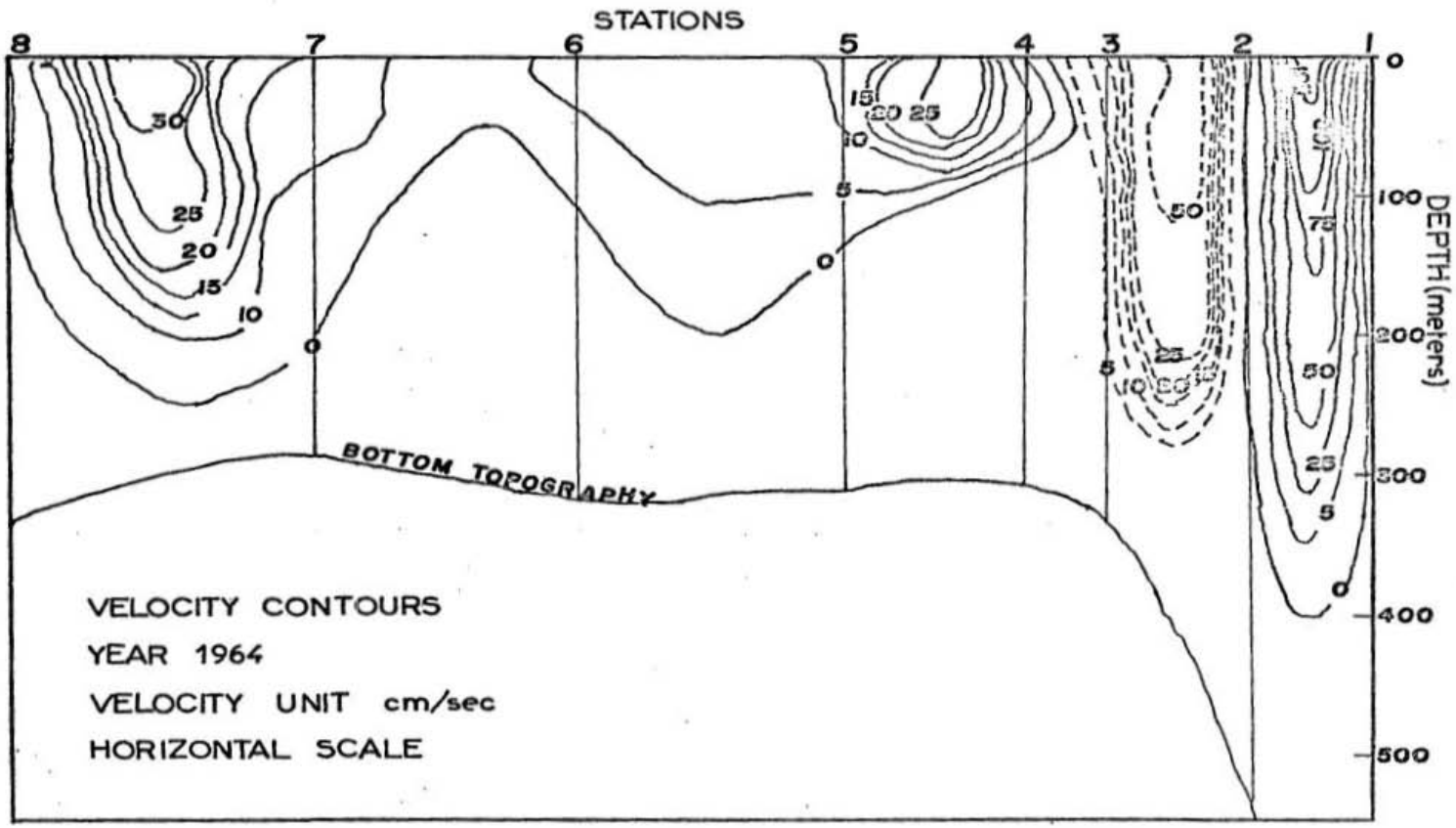

Fig. 28. Velocity contours. (1964).

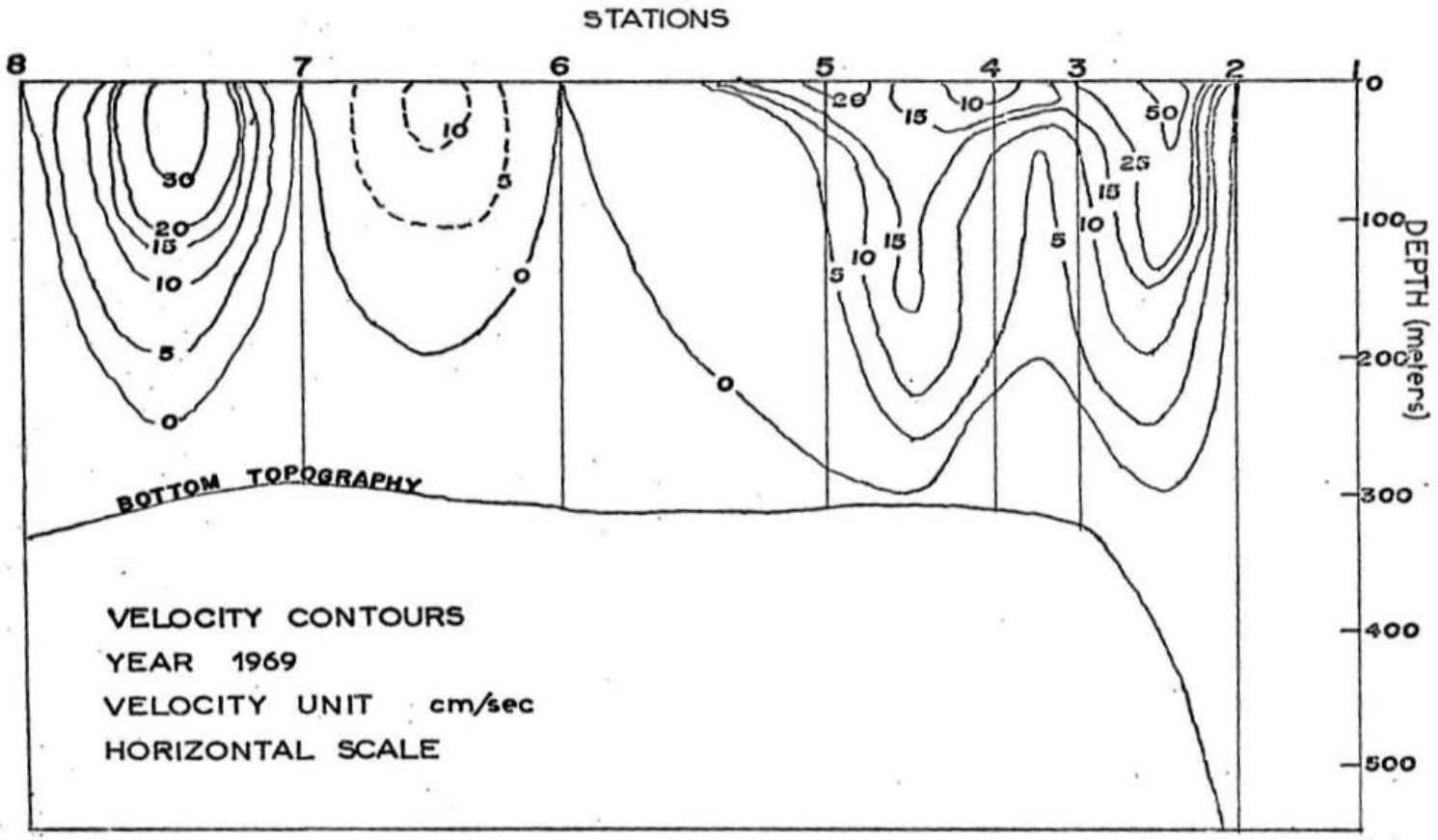

Fig. 29. Velocity contours. (1969).

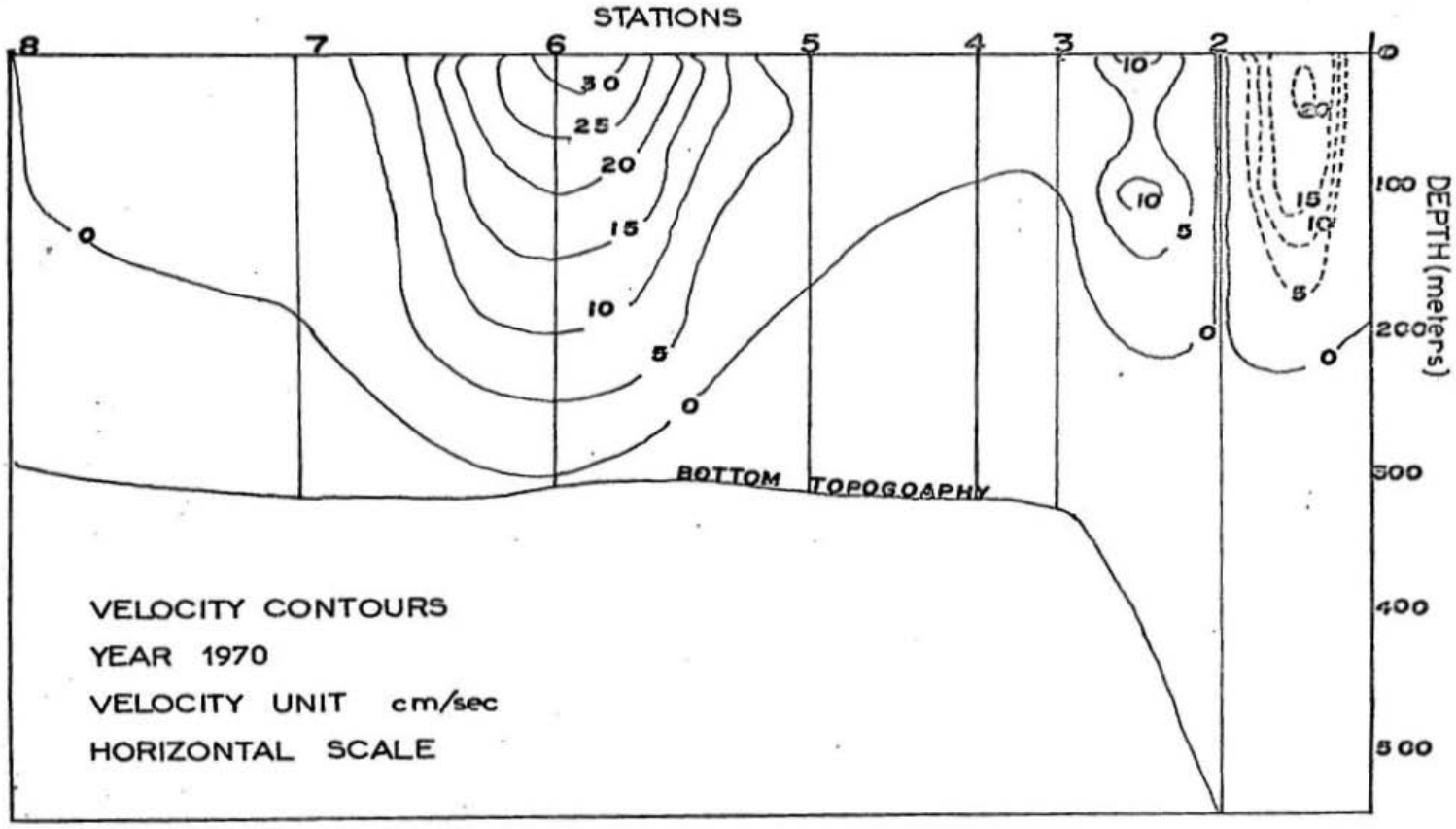

Fig. 30. Velocity contours. (1970).